INTERNATIONAL JOURNAL FOR NUMERICAL METHODS IN FLUIDS, VOL. 9, 783–810 (1989)

INTERNAL WAVE REFLECTIONS AND TRANSMISSIONS ARISING FROM A NON-UNIFORM MESH. PART I: AN ANALYSIS FOR THE CRANK–NICOLSON LINEAR FINITE ELEMENT SCHEME

B. CATHERS

NSW Public Works Department, Hydraulics Laboratory, 110B King Street, Manly Vale, NSW, Australia, 2093

S. BATES

British Gas Corporation, Engineering Research Station, Harvey Combe, Killingworth, PO Box 1LH,
Newcastle upon Tyne NE99 1LH, U.K.

AND

B. A. O'CONNOR

Civil Engineering Department, Liverpool University, Brownlow Street, PO Box 147, Liverpool L69 3BX, U.K.

SUMMARY

This is the first of a series of three related papers dealing with some of the consequences of non-uniform meshes in a numerical model. In this paper the accuracy of the Crank–Nicolson linear finite element scheme, which is applied to the linear shallow water equations, is examined in the context of a single abrupt change in nodal spacing. The (in)accuracy is quantified in terms of reflection and transmission coefficients. An incident wave impinging on the interface between two regions with different nodal spacings is shown to give rise to no reflected waves and *two* transmitted waves. The analysis is verified using three different wavelengths ($2\Delta x$, $4\Delta x$, $8\Delta x$) in three 'hot-start' numerical experiments with a mesh expansion factor of 2 and three experiments with a mesh contraction factor of 1/2. An energy flux analysis based on the concept of group velocity shows that energy is conserved across the interface.

KEY WORDS Non-uniform mesh Wave Reflection/transmission Crank–Nicolson finite elements Fourier analysis

1. INTRODUCTION

A numerical modeller is often required to numerically simulate the hydrodynamics of a limited study area which has boundary conditions which are not well known, or a study area which requires more detail than the neighbouring region(s). Several approaches which can be used to overcome these difficulties include:

(i) *Refinement of the computational grid.* This is accomplished naturally in finite elements, but with finite differences requires more book-keeping in the form of look-up tables for evaluating derivatives.[1]

(ii) *Transforming the co-ordinates.* This method relies on the existence of a suitable transform, which is usually site-specific, to suit the study area.[2]

0271–2091/89/070783–28$14.00
© 1989 by John Wiley & Sons, Ltd.

Received May 1988
Revised September 1988

(iii) *The use of nested grids.* In this method the large-scale prediction is first made on a coarse grid which is completely independent of the nested fine grid computation. Values from the coarse grid are then used to drive the fine grid model. Phillips and Shukla[3] refer to this as '*one-way*' interaction, since only the coarse grid computation can influence the fine grid computation.[4] The main disadvantage of this method is that errors due to the lack of resolution in the coarse grid are fed into the fine grid model along its boundaries.

(iv) *The use of a patchwork model.*[5] In this method calculations on both the coarsely gridded areas and the finely gridded areas are carried out simultaneously. The two meshes are dynamically coupled and there is a '*two-way*' interaction since information from the fine mesh is now incorporated by the coarse mesh and vice versa.

This paper is concerned with point (i) above. However, the techniques of analysis used also apply to point (iv).

Refining (or expanding) a computational mesh is not without its consequences. The purpose of this paper is to investigate some of these effects for the Crank–Nicolson linear finite element scheme based upon the shallow water equations using the consistent mass matrix approach. (Note that the time discretization is effected by the trapezoidal rule, which is somewhat loosely referred to herein, and in other references, as 'Crank–Nicolson'.) Using a Fourier analysis, it is shown how these effects can be quantified (i.e. reflection and transmission coefficients) and lead to an improved understanding of the processes involved when an incident wave or Fourier component encounters a single change in nodal spacing (or mesh size).

The analysis and experiments have been simplified in several respects. The governing equations are the 1D linear shallow water equations. Also, the spatial domain contains only a single change in nodal spacing and the node where this occurs divides the domain into two uniform regions (i.e. 1 and 2) with two different element lengths (Δx_1 and Δx_2). Physically there is no difference between the two regions since they are both characterized by the same depth (i.e. $h_1 = h_2 = h$) and the same fluid ($\rho_1 = \rho_2 = \rho$). The only differences are computational since it is only by the two different element lengths that the two regions can be discerned. The ratio of the element lengths in the two regions will be referred to as the mesh size ratio, i.e. $H' = \Delta x_2/\Delta x_1$.

The consequences of mesh refinement have been largely unexplored until the 1980s. In a series of illuminating papers, Bazant and Celep[6–8] investigated the non-physical wave reflections and inaccurate wave transmissions due to a change in nodal spacing. Their studies were based upon the explicit finite element wave equation scheme using linear and quadratic finite elements for 1D elastic wave propagation in a Lagrangian co-ordinate system.

They quantified the magnitude of the reflected and transmitted waves due to a change in nodal spacing as well as the reflected and transmitted energy fluxes. They concluded that the consistent mass matrix formulation was more accurate than that of lumped mass and that quadratic finite elements performed better than linear finite elements. Interestingly, Bazant[6] found that in the case of a mesh expansion ($\Delta x_1 < \Delta x_2$), the transmitted wave has a larger amplitude than the incident wave but a smaller mean energy flux. He proved, however, that energy was conserved in the limit of $\Delta t \rightarrow 0$ and alluded to the possibility that for larger time steps (especially for an implicit scheme) this might not be the case. It has since been proved by Vichnevetsky[9] that in the general case energy is conserved, and in the present paper it is demonstrated for the Crank–Nicolson FE scheme.

Celep and Bazant[8] also examined the effects of changing the nodal spacing gradually from Δx_1 to Δx_2 through a transition zone. They found that when the element lengths in the transition zone were varied as an arithmetic progression, the results were only marginally better than for a geometric variation. More importantly, they found that for the linear FE wave equation scheme, the effectiveness in mitigating the undesirable reflected waves was insignificant when $0{\cdot}5 > \Delta x_1/\Delta x_2 > 1{\cdot}5$.

Trefethen[10] has examined the results of several interesting systems where the discontinuity between the two regions is the result of using (i) a different FD scheme in each region, (ii) an abrupt change in coefficient or (iii) a mesh refinement. His examples were based upon the transport equation and the second-order wave equation.

Vichnevetsky[11] has carried out an extensive review of a family of numerical schemes (including the Crank–Nicolson linear finite element scheme) with 'computational molecules' involving six points in the x–t plane. One of the main conclusions was that, provided the appropriate energy norm is used, the analyses of many reflection phenomena are independent of the temporal discretization used. This implies, therefore, that such phenomena are adequately investigated by only considering the semi-discrete case.

Worthington[12] has investigated the effect of a single change in mesh size for the Crank–Nicolson and leap–frog finite difference schemes applied to the shallow water equations with the variables for velocity and surface elevation staggered in space. The purpose was to quantify the reflected and transmitted wave amplitudes which would be present in a patchwork model. Consequently, he was interested in the results for two particular mesh size ratios (viz. 3 and 1/3).

One feature which all four of the above-mentioned numerical schemes have in common is that their dispersion relations all increase monotonically. This is in contrast to the Crank–Nicolson linear finite element scheme which is 'hill-shaped' or *concave down*, and the consequences of this fact make its investigation somewhat unusual.

Before the discrete system is investigated, it is of value to investigate a parallel problem in the continuum. For both the discrete and continuum systems, the governing equations are the equations for the conservation of momentum and mass, referred to collectively as the shallow water equations:

$$\frac{\partial u}{\partial t} + g\frac{\partial \eta}{\partial x} = 0, \tag{1}$$

$$\frac{\partial \eta}{\partial t} + h\frac{\partial u}{\partial x} = 0. \tag{2}$$

2. REFLECTION AND TRANSMISSION IN THE CONTINUUM

Unlike the discrete system to be considered next, reflections in the continuum must have a physical basis. They can be caused by a sudden change in geometry. The case to be examined here is of a 1D frictionless prismatic channel with an abrupt change in depth from h_1 to h_2. The subscript '1' is used throughout to refer to the reach upstream of the interface or step, and '2' to the downstream reach. (This is depicted in the inset of Figure 1). When an incident wave impinges on the step in the channel, it gives rise to a reflected wave and a transmitted wave.

Since the system is linear (no convective or friction terms), superposition is valid and the incident waveform can be decomposed into a number of Fourier components. In any analysis, therefore, it is sufficient to consider just one component. The surface elevation or velocity in the upstream section is the result of the incident wave and the reflected wave. This can be expressed in exponential form, where it is understood that only the real part is to be taken, i.e.

$$\eta_1(x, t) = \hat{\eta}\mathrm{e}^{\mathrm{i}(\omega t - \sigma_1 x)} + \beta\hat{\eta}\mathrm{e}^{\mathrm{i}(\omega t + \sigma_1 x)}, \tag{3}$$

$$u_1(x, t) = \sqrt{(g/h_1)}(\hat{\eta}\mathrm{e}^{\mathrm{i}(\omega t - \sigma_1 x)} - \beta\hat{\eta}\mathrm{e}^{\mathrm{i}(\omega t + \sigma_1 x)}), \tag{4}$$

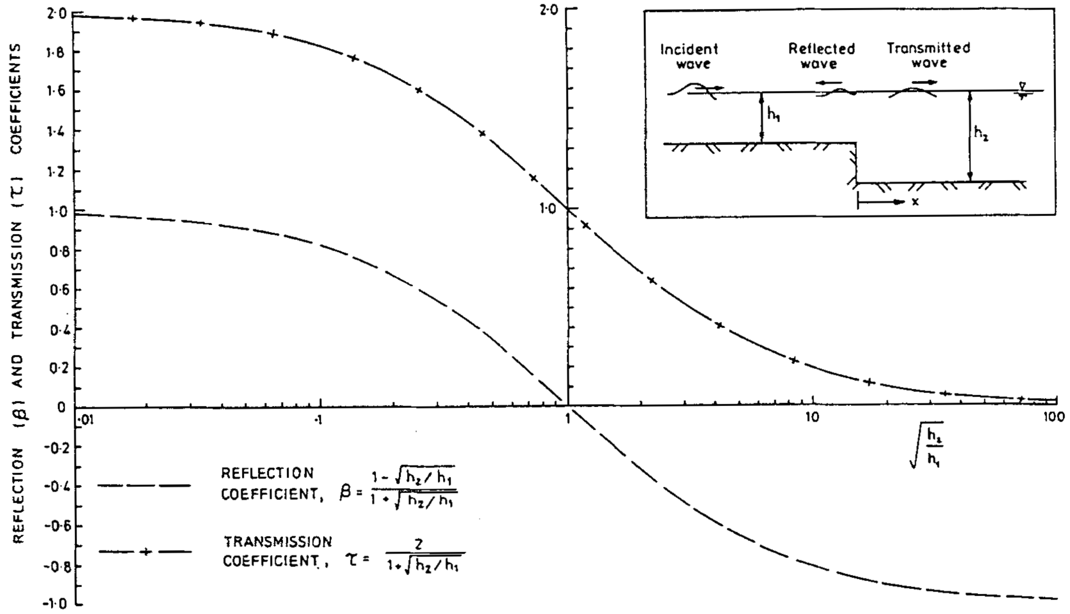

Figure 1. Reflection and transmission coefficients for the shallow water equations due to an abrupt change in depth (h_1 to h_2)

where

η	instantaneous surface elevation
$\hat{\eta}$	amplitude of the surface elevation for the incident wave
ω	angular frequency
σ	wave number
β	reflection coefficient, which in general is complex
x	space co-ordinate measured away from the step in the channel, in the downstream direction
t	time.

In the downstream reach the surface elevation and velocity are given by

$$\eta_2(x, t) = \tau\hat{\eta}\, e^{i(\omega t - \sigma_2 x)}, \tag{5}$$

$$u_2(x, t) = \sqrt{(g/h_2)}\,\tau\hat{\eta}\, e^{i(\omega t - \sigma_2 x)}, \tag{6}$$

where τ is the transmission coefficient, which in general is complex. Substitution of equations (3) and (4) or (5) and (6) into the linear shallow water equations (1) and (2) yields the dispersion relations for the upstream or downstream section, viz. $\omega = \sigma_1 c_1 = \sigma_2 c_2$, where $c_1 = \sqrt{(gh_1)}$ and $c_2 = \sqrt{(gh_2)}$.

In order to quantify the reflected and transmitted waves, it is necessary to supply the internal boundary conditions which are enforced at the step in the channel, where $x = 0$. These boundary conditions are approximate owing to the sudden change in the nature of the fluid motion near the step. Different boundary conditions have been used by various authors. Lamb[13] used the first-order mass flow balance just upstream and downstream of the step as well as the continuity of pressure (and hence surface elevation):

$$\left.\begin{aligned} u_1 h_1 &= u_2 h_2 \qquad (7) \\ \eta_1 &= \eta_2 \qquad (8) \end{aligned}\right\} \text{ at } x = 0 \text{ for all times.}$$

Substitution of equations (3)–(6) into (7) and (8), and requiring that the transmitted wave has the same phase as the incident wave, yields the reflection and transmission coefficients:

$$\beta = \frac{c_1 - c_2}{c_1 + c_2} = \frac{1 - \sqrt{(h_2/h_1)}}{1 + \sqrt{(h_2/h_1)}}, \tag{9}$$

$$\tau = \frac{2c_1}{c_1 + c_2} = \frac{2}{1 + \sqrt{(h_2/h_1)}} = 1 + \beta. \tag{10}$$

Alternatively, for shallow water conditions, the same reflection and transmission coefficients in equations (9) and (10) are also obtained by assuming an energy flux balance at the step as well as a mass flow balance. Svendsen and Jonsson[14] used another approach based on the balance of energy and mass to solve the slightly different problem where the upstream and downstream reaches are joined by a submerged slope (assumed small in length relative to the wavelength) rather than a step. Once again equations (9) and (10) are obtained for shallow water conditions:

The points to note about β and τ in equations (9) and (10) are:

(i) $1 + \beta = \tau$.
(ii) β and τ are both real.
(iii) $-1 < \beta < 1$ and $0 < \tau < 2$.

Some similarities of these three results for the continuum to those in the discrete system (where the discontinuity between the upstream and downstream reaches is only due to numerical reasons, i.e. Δx_1 being different to Δx_2) will become evident.

3. WAVE REFLECTION AND TRANSMISSION IN THE DISCRETE SYSTEM

The discrete system consists of two regions with finite element lengths Δx_1 and Δx_2. The location of the node at the interface of the two regions is taken to be the origin of the x-axis (see Figures 2(a) and 2(b)). Region 1 can be viewed as a domain extending from $x = 0$ to minus infinity ($x \to -\infty$) with a periodic boundary condition at $x = 0$; and similarly for region 2 from $x = 0$ to $x \to +\infty$. Consequently a Fourier analysis is valid and is used in the reflection/transmission analysis.

3.1. Dispersion relations

The dispersion relations will be used to relate the wavelengths present in the two regions.

Since the two regions have different nodal spacings, the operating conditions will also be different. Region 1 is characterized by a Courant number $\mathcal{C}_1 = c\Delta t/\Delta x_1$ and region 2 is characterized by $\mathcal{C}_2 = c\Delta t/\Delta x_2$ (where Δt and Δx are time and space increments). The corresponding dispersion relations at these two Courant numbers are represented in Figures 2(a) and 2(b) for the situations of a mesh refinement and a mesh expansion respectively.

The dispersion relation for the Crank–Nicolson linear finite element scheme is given by

$$\tan\left(\frac{\omega\Delta t}{2}\right) = \frac{1{\cdot}5\mathcal{C}\sin\gamma}{2 + \cos\gamma}, \tag{11}$$

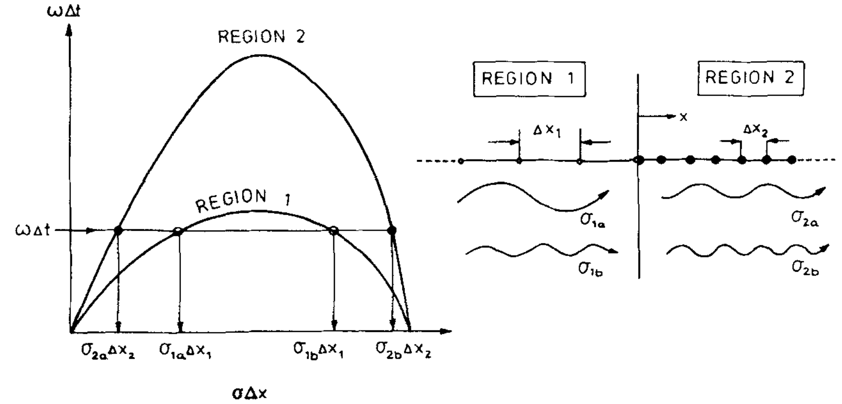

Figure 2(a). Schematics of the dispersion relations of the two regions (above left) and the waves present (above right) for *mesh refinement*, $\Delta x_2 < \Delta x_1$

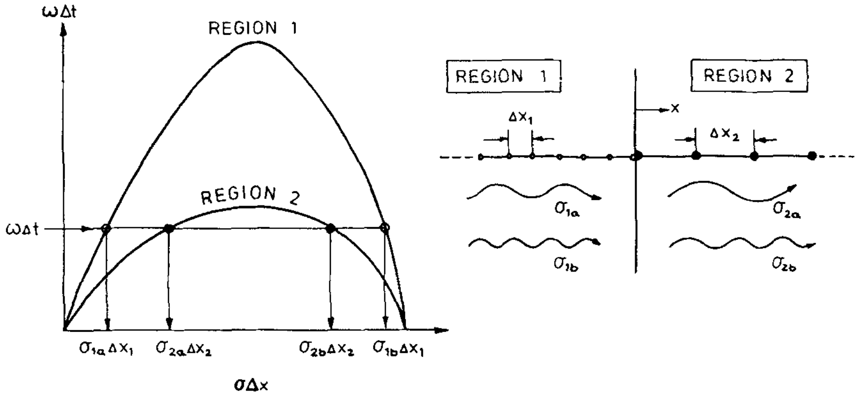

Figure 2(b). Schematics of the dispersion relations of the two regions (above left) and the waves present (above right) for *mesh expansion*, $\Delta x_2 > \Delta x_1$

where $\gamma = \sigma\Delta x$ is the dimensionless wave number. This relation is *concave down* with a maximum frequency $\omega_{\max}$ occurring at $\gamma = 2\pi/3$, irrespective of the Courant number. Platzman[15] refers to such a wave number as a 'folding' wave number. Both infinitely long waves and $2\Delta x$ waves possess zero angular frequency. For frequencies between zero and $\omega_{\max}$, the dispersion relation is cut in two locations corresponding to a relatively long wave number (which has positive group velocity) and a relatively short wave number (which has negative group velocity). These two wave numbers will be termed 'complementary' wave numbers and will be specified as $\gamma_{1a} = \sigma_{1a}\Delta x_1$, $\gamma_{1b} = \sigma_{1b}\Delta x_1$ in region 1 and $\gamma_{2a} = \sigma_{2a}\Delta x_2$, $\gamma_{2b} = \sigma_{2b}\Delta x_2$ in region 2. The wave number γ_{1a} will be used to refer to the *incident* wave number which may have a negative *or* a positive group velocity. Its complementary wave number in region 1 (i.e. γ_{1b}) will have a group velocity with the opposite sign. In region 2, γ_{2a} will refer to the wave number which is associated with the group velocity which has the *same sign* as that for γ_{1a}, and γ_{2b} is its complementary wave number.

For region 1 the dispersion relation is

$$\tan\left(\frac{\omega_1 \Delta t}{2}\right)=\frac{1\cdot 5 \not{C}_1 \sin \gamma_{1\mathrm{a}}}{2+\cos \gamma_{1\mathrm{a}}}=\frac{1\cdot 5 \not{C}_1 \sin \gamma_{1\mathrm{b}}}{2+\cos \gamma_{1\mathrm{b}}}$$

and for region 2

$$\tan\left(\frac{\omega_2 \Delta t}{2}\right)=\frac{1\cdot 5 \not{C}_2 \sin \gamma_{2\mathrm{a}}}{2+\cos \gamma_{2\mathrm{a}}}=\frac{1\cdot 5 \not{C}_2 \sin \gamma_{2\mathrm{b}}}{2+\cos \gamma_{2\mathrm{b}}}.$$

Since the discrete system being analysed is linear, the wave period and hence the wave frequency is the same in both regions. This permits the dispersion relations for the two sides to be linked via the wave frequency $\omega = \omega_1 = \omega_2$. Therefore the two equations above can be combined to give

$$\tan\left(\frac{\omega \Delta t}{2}\right)=\frac{1\cdot 5 \not{C}_1 \sin \gamma_{1\mathrm{a}}}{2+\cos \gamma_{1\mathrm{a}}}=\frac{1\cdot 5 \not{C}_1 \sin \gamma_{1\mathrm{b}}}{2+\cos \gamma_{1\mathrm{b}}}$$
$$=\frac{1\cdot 5 \not{C}_2 \sin \gamma_{2\mathrm{a}}}{2+\cos \gamma_{2\mathrm{a}}}=\frac{1\cdot 5 \not{C}_2 \sin \gamma_{2\mathrm{b}}}{2+\cos \gamma_{2\mathrm{b}}}. \qquad (12)$$

Equation (12) permits $\gamma_{1\mathrm{a}}$, $\gamma_{1\mathrm{b}}$, $\gamma_{2\mathrm{a}}$ and $\gamma_{2\mathrm{b}}$ to be related to each other. In all the analyses which follow, the incident wave impinges on the interfacial node at $x=0$ from region 1. If the incident wavelength $L_{1\mathrm{a}}=2\pi/\sigma_{1\mathrm{a}}$ exceeds $3\Delta x_1$, then both phase and energy are directed towards the interface. However, if this wavelength is less than $3\Delta x_1$, then the energy flux is away from the interface and the wave is incident only in the sense of phase.

Using equation (12), the relations between wave numbers in the same region will be established, i.e. between γ_a and γ_b. After this the relations between wave numbers in different regions will be found, i.e. between γ_1 and γ_2.

3.2. Calculation of wave numbers in the same region

In this section the complementary wave numbers will be related, i.e. γ_a and γ_b. In region 1 this means that the relation between $\gamma_{1\mathrm{a}}$ and $\gamma_{1\mathrm{b}}$ will be determined, or for region 2, $\gamma_{2\mathrm{a}}$ and $\gamma_{2\mathrm{b}}$ will be related. Equating the second and third terms (or the fourth and fifth terms) in equation (12) gives

$$\frac{\sin \gamma_\mathrm{a}}{2+\cos \gamma_\mathrm{a}}=\frac{\sin \gamma_\mathrm{b}}{2+\cos \gamma_\mathrm{b}}.$$

Simplifying the above leads to

$$3=\tan\left(\frac{\gamma_\mathrm{a}}{2}\right)\tan\left(\frac{\gamma_\mathrm{b}}{2}\right). \qquad (13)$$

Equation (13) permits $\gamma_{1\mathrm{b}}$ to be found from $\gamma_{1\mathrm{a}}$, $\gamma_{2\mathrm{b}}$ from $\gamma_{2\mathrm{a}}$ and vice versa.

3.3. Calculation of the real wave numbers in different regions

In this section γ_2 will be found in terms of γ_1. It is understood that the incident wave number γ_1 is real.

From equation (12)

$$\tan\left(\frac{\omega \Delta t}{2}\right)=\frac{1\cdot 5 \not{C}_1 \sin \gamma_1}{2+\cos \gamma_1}=\frac{1\cdot 5 \not{C}_2 \sin \gamma_2}{2+\cos \gamma_2}. \qquad (14)$$

Letting

$$H' = \frac{\Delta x_2}{\Delta x_1} = \frac{\text{₵}_1}{\text{₵}_2} \quad \text{and} \quad R_1 = \frac{H' \sin \gamma_1}{2 + \cos \gamma_1} = \left(\frac{2}{3\text{₵}_2}\right) \tan\left(\frac{\omega \Delta t}{2}\right),$$

equation (14) becomes

$$\tan\left(\frac{\gamma_2}{2}\right) = \frac{1 \pm \sqrt{(1 - 3R_1^2)}}{R_1}. \tag{15}$$

This equation shows that for a given incident wave number γ_1, there are two possible wave numbers in the downstream region 2, which are γ_{2a} and γ_{2b}.

By following the convention for defining the various wave numbers which was detailed in the previous section, the following equations are derived from equation (15).

If $2\pi/(\gamma_{1a}) < 3$, i.e. $L_{1a} < 3\Delta x_1$, then

$$\tan\left(\frac{\gamma_{2a}}{2}\right) = \frac{1 + \sqrt{(1 - 3R_1^2)}}{R_1} \tag{16}$$

and

$$\tan\left(\frac{\gamma_{2b}}{2}\right) = \frac{1 - \sqrt{(1 - 3R_1^2)}}{R_1}. \tag{17}$$

If $2\pi/(\gamma_{1a}) > 3$, i.e. $L_{1a} > 3\Delta x_1$, then

$$\tan\left(\frac{\gamma_{2a}}{2}\right) = \frac{1 - \sqrt{(1 - 3R_1^2)}}{R_1} \tag{18}$$

and

$$\tan\left(\frac{\gamma_{2b}}{2}\right) = \frac{1 + \sqrt{(1 - 3R_1^2)}}{R_1}. \tag{19}$$

If $2\pi/(\gamma_{1a}) = 3$, i.e. $L_{1a} = 3\Delta x_1$, then

$$\tan\left(\frac{\gamma_{2a}}{2}\right) = \tan\left(\frac{\gamma_{2b}}{2}\right) = \frac{1}{R_1}. \tag{20}$$

Equations (16)–(20) relate the wave numbers in the different regions. These equations contain the discriminant $\sqrt{(1 - 3R_1^2)}$, and the possibility of it turning complex for certain values of R_1 needs to be investigated.

From equation (15), γ_2 is real provided $1 - 3R_1^2 \geq 0$, i.e.

$$\frac{1}{H'} \geq \frac{\sqrt{3} \sin \gamma_1}{2 + \cos \gamma_1}. \tag{21}$$

The right-hand side of this inequality has a maximum value of unity at $\gamma_1 = 2\pi/3$. The inequality (21) is always satisfied for $H' \leq 1$ irrespective of γ_1. Thus, in the case of *mesh refinement* ($H' \leq 1$), γ_2 in equations (16)–(20) is always real.

In the case of a *mesh expansion*, the conditions that γ_2 is real are also determined from the inequality (21):

$$\tan(\gamma_1/2) \geqslant \sqrt{3}[H' + \sqrt{(H'^2 - 1)}], \tag{22a}$$

$$\tan(\gamma_1/2) \leqslant \sqrt{3}(H' - \sqrt{(H'^2 - 1)}]. \tag{22b}$$

These relations shows that in the case of a *mesh expansion*, whether γ_2 is real or complex depends on both the mesh size ratio H' and γ_1 (see Figure 1 of Part III of this series). γ_2 is real provided the inequalities (22) are satisfied. For example, when $H' = 2$, γ_2 is real so long as

$$\gamma_1 \geqslant 2{\cdot}835 \quad \text{or} \quad \gamma_1 \leqslant 0{\cdot}869,$$

i.e. $2{\cdot}217 \geqslant N_{x1} > 7{\cdot}230$, where $N_{x1} = (L/\Delta x)_1$ and L_1 is the wavelength in region 1. Incident wavelengths in region 1 between $2{\cdot}217\,\Delta x_1$ and $7{\cdot}230\,\Delta x_1$ will give rise to complex wave numbers in region 2.

If the inequalities (22) are not satisfied then γ_2 will be complex, and this corresponds to an evanescent wave which is damped (or growing) exponentially in space. This case will be dealt with in Part III of this series. It is seen, therefore, that in the case of a mesh expansion it is not a simple matter of arbitrarily selecting a (real) incident wave number in region 1 and using equations (16)–(20) to determine the complementary wave numbers in region 2. If $1-3R_1^2 < 1$, the wave numbers in region 2 are complex. A mesh refinement on the other hand does not have these difficulties, since for every real wave number γ_1 there are two real complementary wave numbers in region 2.

The differences between a mesh refinement and mesh expansion with regard to wave numbers can be made clearer by referring to the dispersion relations (see Figures 2(a) and 2(b)). It will be shown in Part III that, provided the frequency of oscillation at a boundary is less than or equal to the maximum frequency of the dispersion relation, the wave numbers will be real. If, however, the frequency of oscillation at the boundary exceeds the maximum frequency of the dispersion relation, the wave numbers will be complex. Figure 2(a) refers to the case of a *mesh refinement*; because $\not{C}_2 > \not{C}_1$, the dispersion relation for region 2 encloses that for region 1. It is obvious that the intersection of the dispersion relation for region 1 in one or two points for a particular frequency is a sufficient condition that the region 2 dispersion relation will also be intersected in two points. Therefore, provided the wave numbers in region 1 are real, it automatically follows that the wave numbers in region 2 will also be real. If $\omega_{\max 1}$ and $\omega_{\max 2}$ refer to the maximum frequencies of the dispersion relations for regions 1 and 2, and ω refers to the frequency of oscillation at a boundary or interface, it can be seen from Figure 2(a) that there are three possible ranges for ω in the case of a *mesh refinement*:

(i) $\omega < \omega_{\max 1} < \omega_{\max 2}$—all wave numbers in both regions are real
(ii) $\omega_{\max 1} < \omega < \omega_{\max 2}$—incident or region 1 wave numbers are complex, region 2 wave numbers are real
(iii) $\omega_{\max 1} < \omega_{\max 2} < \omega$—all wave numbers in both regions are complex.

Figure 2(b) depicts the situation for a *mesh expansion*. The three ranges for ω are:

(i) $\omega < \omega_{\max 2} < \omega_{\max 1}$—all wave numbers in both regions are real
(ii) $\omega_{\max 2} < \omega < \omega_{\max 1}$—incident or region 1 wave numbers are real, region 2 wave numbers are complex
(iii) $\omega_{\max 2} < \omega_{\max 1} < \omega$—all wave numbers in both regions are complex.

In summary, it is seen that in the case of *mesh refinement*, real incident wave numbers guarantee real wave numbers in region 2. For a *mesh expansion*, however, real incident wave numbers do not necessarily give rise to real wave numbers in region 2.

An interesting point about the kinematic part of the analysis is how relatively long wavelengths in region 1 can give rise to significantly shorter wavelengths in region 2 and vice versa. Thus in spite of the system being linear, there is a false energy cascade or jump from short wavelengths to long wavelengths and vice versa, which has its origins in the change in nodal spacing. For $H' = 1/2$

and 2, Figure 3 shows how the wavelength contracts and/or expands after passing through a change in mesh size. It has been shown how an incident wave with dimensionless wave number γ_{1a} gives rise to wave numbers γ_{2a} and γ_{2b} in region 2. γ_{2a} refers to the 'physical' wave number and γ_{2b} to the 'aliased' or 'parasitic' wave number, since as the incident wavelength $L_{1a} \to \infty$ then $L_{2a} \to \infty$ also, but $L_{2b} \to 2\Delta x_2$, i.e. the physical transmitted wavelength tends to the incident wavelength but the aliased transmitted wavelengths become very short and unrealistic. It has been shown how for a mesh expansion of $\Delta x_2/\Delta x_1 = 2$ there is a range of incident wavelengths (i.e. $2{\cdot}217 < L_{1a}/\Delta x_1 < 7{\cdot}230$) which give rise to complex wavelengths in region 2. This is shown as the dashed line in Figure 3 and will be considered further in Part III of this series of papers. If other values of H' were plotted, it could be seen how the greater the change in mesh size, the greater the distortion of the physical transmitted wavelength with respect to the incident wavelength.

Now that the kinematic aspect of the reflection/transmission analysis is complete, it is possible to carry out a dynamic analysis which permits the calculation of the reflection and transmission coefficients.

3.4. *Reflection/transmission analysis due to a change in mesh size*

The first step in the analysis is to assume a solution. As was done for the continuum, it is only necessary to consider one Fourier component for the incident wave, since the system is linear and any general incident waveform can be built up by superposition. By taking cognisance of the form of the dispersion relation (and this is the crux of the analysis), allowance must be made for two (and not one) reflected waves and two (rather than one) transmitted waves. This is because an oscillation at a boundary (such as the interfacial node) can give rise to two waves with complementary wavelengths. Figure 4 details the waves present in the system.

The reflection coefficients of the two reflected waves with wave numbers σ_{1a} and σ_{1b} are β_1 and β_2 respectively, while the transmission coefficients of the two transmitted waves with wave-numbers σ_{2a} and σ_{2b} are τ_1 and τ_2 respectively.

The interfacial node at $x = 0$ is atypical of both regions and therefore needs its amplitude (α) to be assigned independently.

In region 1, where $x < 0$, the combined instantaneous velocity and surface elevation are given by

$$u(x, t) = \hat{u}\,\mathrm{e}^{\mathrm{i}(\omega t - \sigma_{1a} x)} - \beta_1 \hat{u}\,\mathrm{e}^{\mathrm{i}(\omega t + \sigma_{1a} x)} - \beta_2 \hat{u}\,\mathrm{e}^{\mathrm{i}(\omega t + \sigma_{1b} x)}, \tag{23}$$

$$\eta(x, t) = \surd(h/g)(\hat{u}\,\mathrm{e}^{\mathrm{i}(\omega t - \sigma_{1a} x)} + \beta_1 \hat{u}\,\mathrm{e}^{\mathrm{i}(\omega t + \sigma_{1a} x)} + \beta_2 \hat{u}\,\mathrm{e}^{\mathrm{i}(\omega t + \sigma_{1b} x)}); \tag{24}$$

in region 2, where $x > 0$, they are

$$u(x, t) = \tau_1 \hat{u}\,\mathrm{e}^{\mathrm{i}(\omega t - \sigma_{2a} x)} + \tau_2 \hat{u}\,\mathrm{e}^{\mathrm{i}(\omega t - \sigma_{2b} x)}, \tag{25}$$

$$\eta(x, t) = \surd(h/g)(\tau_1 \hat{u}\,\mathrm{e}^{\mathrm{i}(\omega t - \sigma_{2a} x)} + \tau_2 \hat{u}\,\mathrm{e}^{\mathrm{i}(\omega t - \sigma_{2b} x)}); \tag{26}$$

and at the interfacial node, where $x = 0$, they are

$$u(0, t) = \alpha \hat{u}\,\mathrm{e}^{\mathrm{i}\omega t}, \tag{27}$$

$$\eta(0, t) = \surd(h/g)\alpha \hat{u}\,\mathrm{e}^{\mathrm{i}\omega t}. \tag{28}$$

The linear shallow water equations (1) and (2) are satisfied by all three sets of assumed solutions above. Equations (23)–(28) contain five unknowns. These are the reflection coefficients (β_1 and β_2), the transmission coefficients (τ_1 and τ_2) and α. All unknowns are in general complex, which means that phase lags or leads with respect to the incident wave are automatically included.

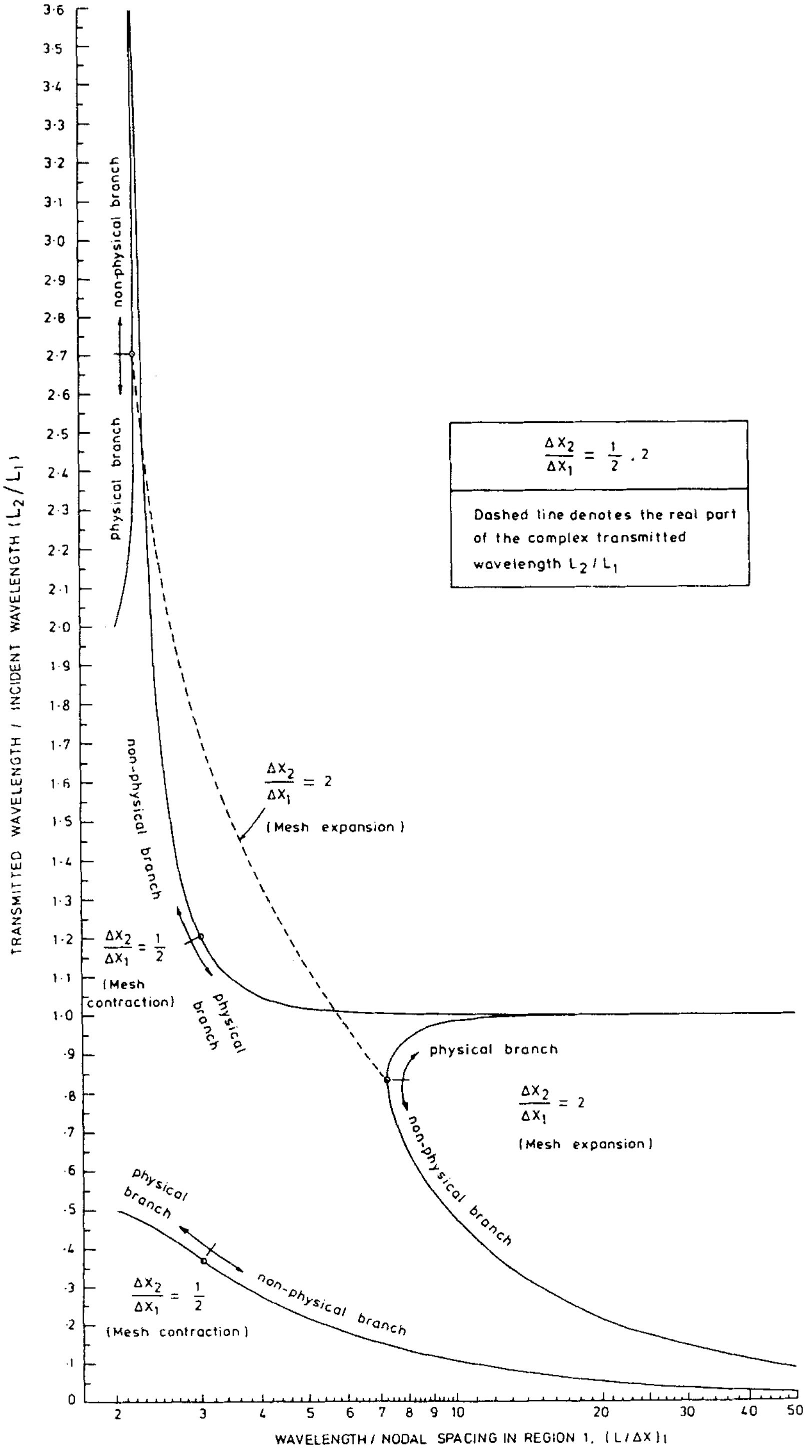

Figure 3. Transmitted/incident wavelength (L_2/L_1) due to a single mesh size change (Δx_1 to Δx_2) for the Crank–Nicolson linear finite element scheme applied to the shallow water equations

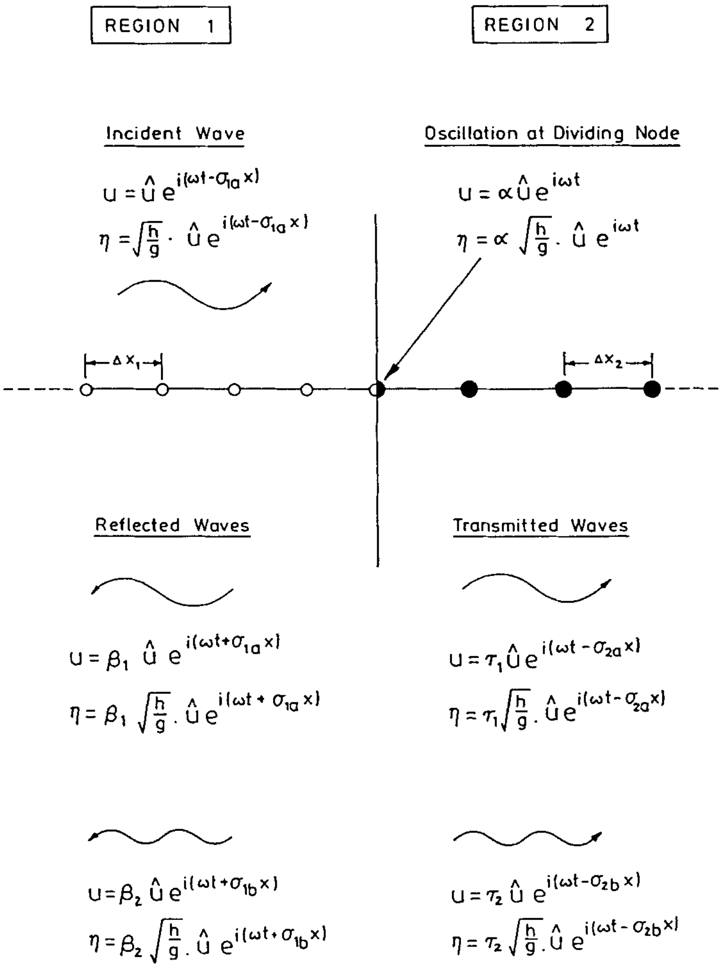

Figure 4. Waves present in the system for the Crank–Nicolson linear finite element scheme applied to the shallow water equations

Application of the Crank–Nicolson linear finite element method centred about node j to the momentum equation(s) gives

$$\frac{\Delta x_{j-1}}{6}\left[\left(\frac{u^{n+1}-u^n}{\Delta t}\right)_{j-1}+2\left(\frac{u^{n+1}-u^n}{\Delta t}\right)_j\right]+\frac{\Delta x_j}{6}\left[2\left(\frac{u^{n+1}-u^n}{\Delta t}\right)_j+\left(\frac{u^{n+1}-u^n}{\Delta t}\right)_{j+1}\right]$$
$$+\frac{g}{4}(\eta_{j+1}-\eta_{j-1})^{n+1}+\frac{g}{4}(\eta_{j+1}-\eta_{j-1})^n=0, \qquad (29)$$

where

Δx_j distance between nodes j and $j+1$
j spatial index
n temporal index.

In the reflection/transmission problem, j takes on the values $-2, -1, 0, 1, 2$, which correspond to the nodal locations at $x = -2\Delta x_1, -\Delta x_1, 0, \Delta x_2, 2\Delta x_2$.

The continuity equation analogous to equation (29) is easily found by interchanging the u's and the η's, and by replacing the g's by h's.

3.4.1. Momentum and mass equations centred about $x = -\Delta x_1$.

Since there are five unknowns, five equations are needed. The first two equations come from applying the finite element operator centred about the node $j = -1$ to the mass and momentum equations. The momentum equation will be considered first. When $j = -1$, equation (29) becomes

$$\frac{1}{6}\left[\left(\frac{u^{n+1}-u^n}{\Delta t}\right)_{-2} + 4\left(\frac{u^{n+1}-u^n}{\Delta t}\right)_{-1} + \left(\frac{u^{n+1}-u^n}{\Delta t}\right)_0\right] + \frac{g}{2}\left[\left(\frac{\eta_0-\eta_{-2}}{2\Delta x_1}\right)^{n+1} + \left(\frac{\eta_0-\eta_{-2}}{2\Delta x_1}\right)^{n}\right] = 0. \tag{30}$$

The expressions for the assumed solution (equations (23)–(28)) appropriate to either region 1 (for $j < 0$), region 2 (for $j > 0$) or the interface ($j = 0$) can be substituted into equation (30) to give, after simplifying,

$$\frac{4}{\not{C}_1}\left(\frac{\lambda-1}{\lambda+1}\right)(e^{2i\gamma_{1a}} - \beta_1 e^{-2i\gamma_{1a}} - \beta_2 e^{-2i\gamma_{1b}} + 4e^{i\gamma_{1a}} - 4\beta_1 e^{-i\gamma_{1a}} - 4\beta_2 e^{i\gamma_{1b}} + \alpha) + (\alpha - e^{2i\gamma_{1a}} - \beta_1 e^{-2i\gamma_{1a}} - \beta_2 e^{-2i\gamma_{1b}}) = 0, \tag{31}$$

where

$$\not{C}_1 = \sqrt{(gh)}\Delta t/\Delta x_1, \qquad \lambda = e^{i\omega\Delta t}, \qquad \gamma_{1a} = \sigma_{1a}\Delta x_1, \qquad \gamma_{1b} = \sigma_{1b}\Delta x_1.$$

Similarly, application of the continuity equation about $x = -\Delta x_1$ results in the following equation, which differs from (31) only in that the signs of the terms involving reflections are reversed:

$$\frac{4}{\not{C}_1}\left(\frac{\lambda-1}{\lambda+1}\right)(e^{2i\gamma_{1a}} + \beta_1 e^{-2i\gamma_{1a}} + \beta_2 e^{-2i\gamma_{1b}} + 4e^{i\gamma_{1a}} + 4\beta_1 e^{-i\gamma_{1a}} + 4\beta_2 e^{-i\gamma_{1b}} + \alpha) + (\alpha - e^{2i\gamma_{1a}} + \beta_1 e^{-2i\gamma_{1a}} + \beta_2 e^{-2i\gamma_{1b}}) = 0. \tag{32}$$

3.4.2. Momentum and mass equations centred about $x = 0$.

The momentum equation to be considered next is found by setting $j = 0$ in equation (29) to give

$$\frac{\Delta x_1}{6}\left[\left(\frac{u^{n+1}-u^n}{\Delta t}\right)_{-1} + 2\left(\frac{u^{n+1}-u^n}{\Delta t}\right)_0\right] + \frac{\Delta x_2}{6}\left[2\left(\frac{u^{n+1}-u^n}{\Delta t}\right)_0 + \left(\frac{u^{n+1}-u^n}{\Delta t}\right)_1\right] + \frac{g}{4}(\eta_1-\eta_{-1})^{n+1} + \frac{g}{4}(\eta_1-\eta_{-1})^{n} = 0. \tag{33}$$

Substitution of the appropriate assumed solutions (equations (23)–(28)) into equation (33) leads to

$$\frac{4}{6\not{C}_1}\left(\frac{\lambda-1}{\lambda+1}\right)(e^{i\gamma_{1a}} - \beta_1 e^{-i\gamma_{1a}} - \beta_2 e^{-i\gamma_{1b}} + 2\alpha) + \frac{4}{6\not{C}_2}\left(\frac{\lambda-1}{\lambda+1}\right)(2\alpha + \tau_1 e^{-i\gamma_{2a}} + \tau_2 e^{-i\gamma_{2b}}) + (\tau_1 e^{-i\gamma_{2a}} + \tau_2 e^{-i\gamma_{2b}} - e^{i\gamma_{1a}} - \beta_1 e^{-i\gamma_{1a}} - \beta_2 e^{-i\gamma_{1b}}) = 0, \tag{34}$$

where $\not{C}_2 = c\Delta t/\Delta x_2$. Similarly, the continuity equation centred about $x = 0$ yields

$$\frac{4}{6\not{C}_1}\left(\frac{\lambda-1}{\lambda+1}\right)(e^{i\gamma_{1a}} + \beta_1 e^{-i\gamma_{1a}} + \beta_2 e^{-i\gamma_{1b}} + 2\alpha) + \frac{4}{6\not{C}_2}\left(\frac{\lambda-1}{\lambda+1}\right)(2\alpha + \tau_1 e^{-i\gamma_{2a}} + \tau_2 e^{-i\gamma_{2b}})$$
$$+ (\tau_1 e^{-i\gamma_{2a}} + \tau_2 e^{-i\gamma_{2b}} - e^{i\gamma_{1a}} + \beta_1 e^{-i\gamma_{1a}} + \beta_2 e^{-i\gamma_{1b}}) = 0. \qquad (35)$$

3.4.3. Momentum or continuity equation centred about $x = \Delta x_2$. The fifth and final equation is obtained by centring the momentum equation about the node at $x = \Delta x_2$. (The continuity equation is redundant since it yields exactly the same equation and will therefore be omitted.) When $j = 1$, equation (29) becomes

$$\frac{1}{6}\left[\left(\frac{u^{n+1}-u^n}{\Delta t}\right)_0 + 4\left(\frac{u^{n+1}-u^n}{\Delta t}\right)_1 + \left(\frac{u^{n+1}-u^n}{\Delta t}\right)_2\right] + \frac{g}{2}\left[\left(\frac{\eta_2-\eta_0}{2\Delta x_1}\right)^{n+1} + \left(\frac{\eta_2-\eta_0}{2\Delta x_1}\right)^{n}\right] = 0. \qquad (36)$$

Substitution of equations (25)–(28) into the above equation leads to

$$\frac{4}{6\not{C}_1}\left(\frac{\lambda-1}{\lambda+1}\right)(\alpha + 4\tau_1 e^{-i\gamma_{2a}} + 4\tau_2 e^{-i\gamma_{2b}} + \tau_1 e^{-2i\gamma_{2a}} + \tau_2 e^{-2i\gamma_{2b}})$$
$$+ (\tau_1 e^{-2i\gamma_{2a}} + \tau_2 e^{-2i\gamma_{2b}} - \alpha) = 0. \qquad (37)$$

3.5. Solution of the equations

The five equations in the five unknowns (α, β_1, β_2, τ_1, τ_2) are (31), (32), (34), (35) and (37). By manipulation and substitution of the equation

$$\frac{\lambda-1}{\lambda+1} = i\left(\frac{1{\cdot}5\not{C}_1 \sin\gamma_{1a}}{2+\cos\gamma_{1a}}\right),$$

which is a form of the dispersion relation, the following solutions are obtained:

$$\alpha = 1 + 0i, \qquad \beta_1 = \beta_2 = 0 + 0i, \qquad (38)$$

$$\tau_1 = 0{\cdot}5\left[1 + \frac{\left(\dfrac{1+2\cos\gamma_{1a}}{2+\cos\gamma_{1a}}\right)}{\left(\dfrac{1+2\cos\gamma_{2a}}{2+\cos\gamma_{2a}}\right)}\right], \qquad (39)$$

$$\tau_2 = 0{\cdot}5\left[1 - \frac{\left(\dfrac{1+2\cos\gamma_{1a}}{2+\cos\gamma_{1a}}\right)}{\left(\dfrac{1+2\cos\gamma_{2a}}{2+\cos\gamma_{2a}}\right)}\right]. \qquad (40)$$

This solution is quite unexpected, because it means that there are no reflected waves!

3.6. Discussion of the solutions to the equations

The transmission coefficients τ_1 and τ_2 given by equations (39) and (40) are plotted in Figures 5–7 for mesh expansion ratios $H' = 1{\cdot}01$ and 2, 1·1 and 3, 3/2 and 5, while Figures 8 and 9

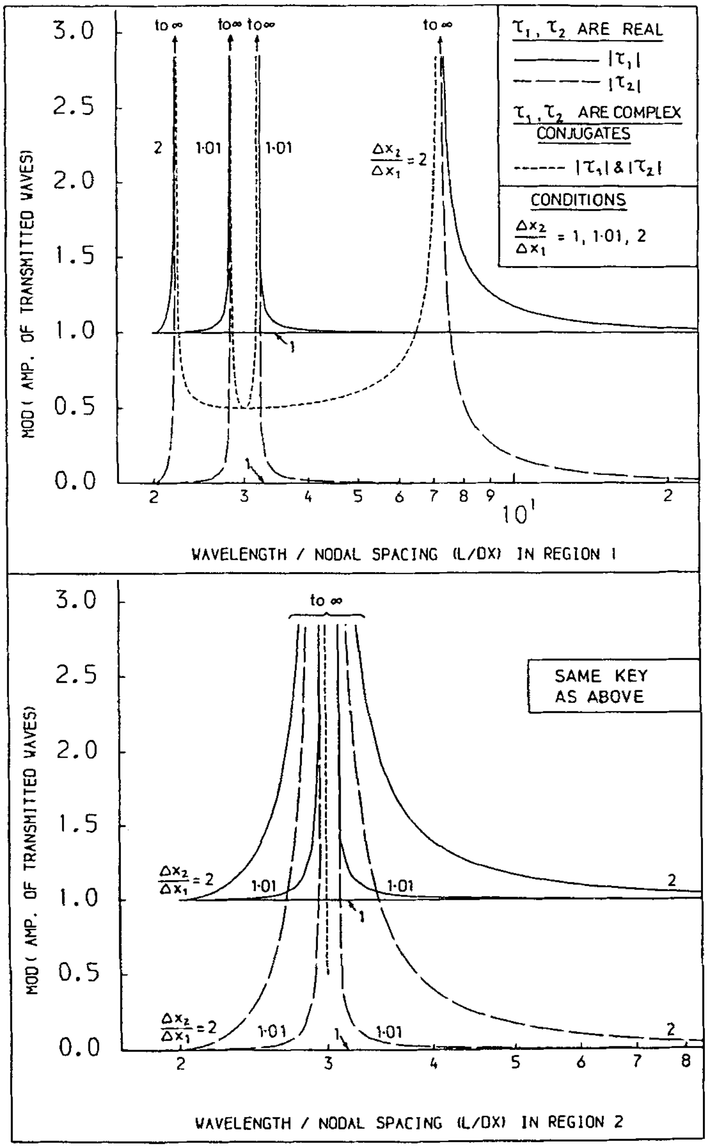

Figure 5. Transmitted waves due to a single change in mesh size (Δx_1 to Δx_2): Crank–Nicolson finite elements applied to the shallow water equations: $\Delta x_2/\Delta x_1 \geqslant 1$ (mesh expansion): $\Delta x_2/\Delta x_1 = 1, 1{\cdot}01, 2$

apply for the mesh contraction ratios to 0·99, 2/3, 1/3 and 0·9, 0·5, 0·2. The following points are noteworthy:

1. The effect of the mesh size ratio H' is not contained explicitly in the expressions for τ_1 and τ_2, but rather implicitly in the relationship between γ_{1a} and γ_{2a}.
2. The absolute values of the Courant numbers in regions 1 and 2 do not affect the transmission coefficients τ_1 and τ_2. (The relative value, i.e. $\mathcal{C}_1/\mathcal{C}_2 = H'$, enters implicitly as noted above.)
3. $\tau_1 + \tau_2 = 1 + 0\mathrm{i}$—see equations (39) and (40).
4. There is a discontinuity in τ_1 and τ_2 as γ_{2a} approaches $2\pi/3$ (i.e. as $L_{2a} \rightarrow 3\Delta x_2$).

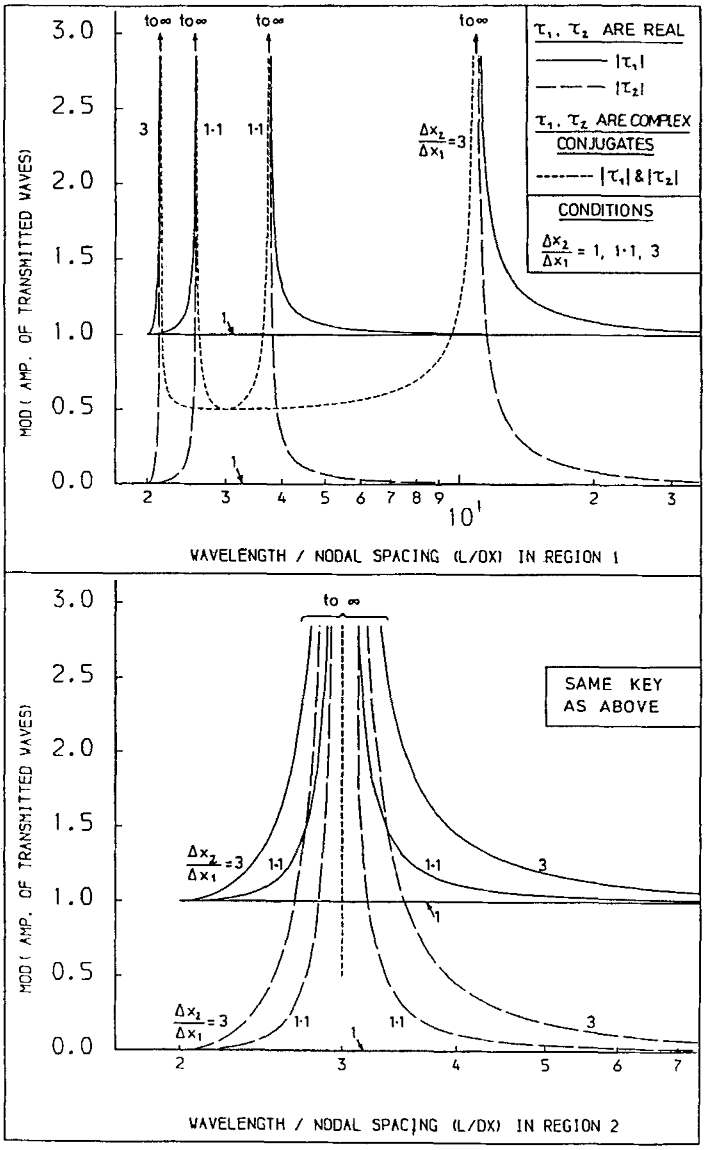

Figure 6. Transmitted waves due to a single change in mesh size (Δx_1 to Δx_2): Crank–Nicolson finite elements applied to the shallow water equations: $\Delta x_2/\Delta x_1 \geqslant 1$ (mesh expansion): $\Delta x_2/\Delta x_1 = 1, 1{\cdot}1, 3$

5. As the incident wave becomes very long (i.e. $L_{1a} \rightarrow \infty$), the change in mesh size becomes insignificant with respect to the wavelength, and $\tau_1 \rightarrow 1 + 0\mathrm{i}$ and $\tau_2 \rightarrow 0 + 0\mathrm{i}$. Thus τ_1, which is associated with γ_{2a}, can be regarded as the transmitted wave which is physically meaningful and τ_2, which is associated with the 'complementary' wave number γ_{2b}, as a 'spurious' or non-physical transmitted wave.
6. As soon as the mesh deviates from being uniform (say $H' = 1{\cdot}01$ or $0{\cdot}99$), Figures 5 and 8 show that the effects on τ_1 and τ_2 are large for a narrow band of wavelengths. At lower or higher mesh size ratios, the effects on τ_1 and τ_2 are more pronounced for a broader band of wavelengths.

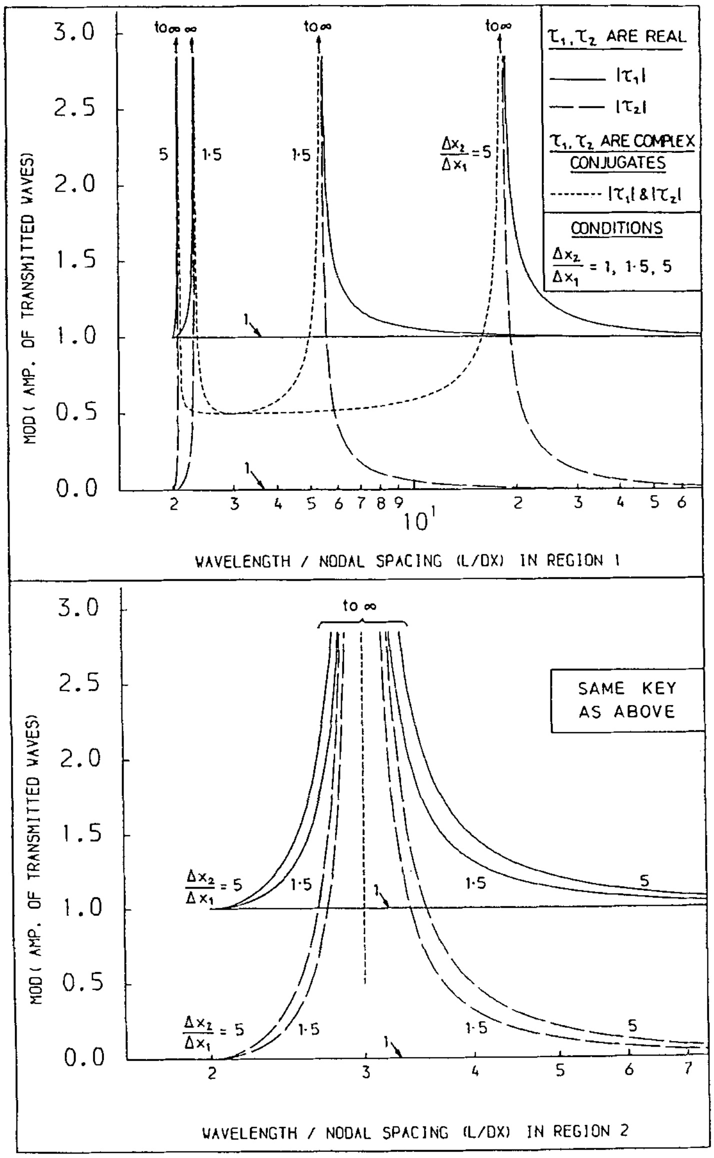

Figure 7. Transmitted waves due to a single change in mesh size (Δx_1 to Δx_2): Crank–Nicolson finite elements applied to the shallow water equations: $\Delta x_2/\Delta x_1 \geqslant 1$ (mesh expansion): $\Delta x_2/\Delta x_1 = 1, 1{\cdot}5, 5$

7. For mesh refinement, $|\tau_1|$ and $|\tau_2| \leqslant 1$ (see Figures 8 and 9), whereas for mesh expansion, $|\tau_1|$ and $|\tau_2| \geq 1$ (see Figures 5–7). (The dashed sections in Figures 5–7 relate to the occurrence of complex wave numbers and evanescent waves in the downstream region. This case is considered in detail in Part III of this series of papers.)

3.7. *Numerical experiments*

In order to check the analyses, a series of six numerical tests was carried out with two different mesh size ratios using three different wavelengths. The mesh size ratios used were $H' = 2$ for mesh

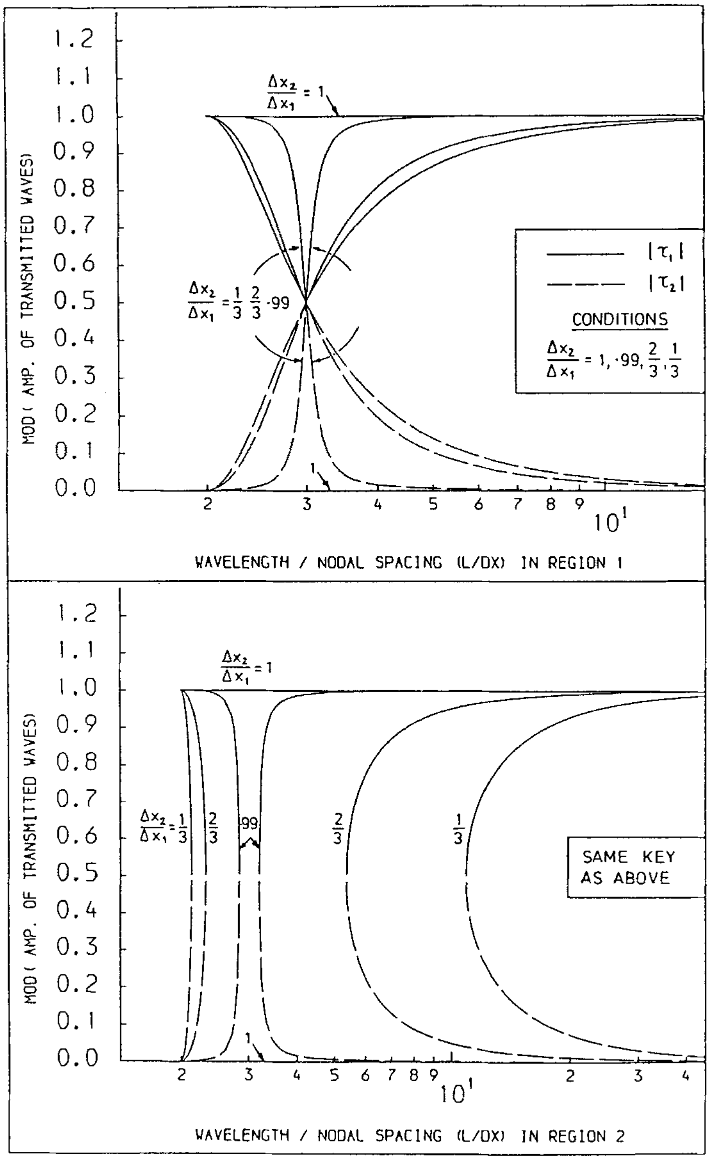

Figure 8. Transmitted waves due to a single change in mesh size (Δx_1 to Δx_2): Crank–Nicolson finite elements applied to the shallow water equations: $\Delta x_2/\Delta x_1 \leqslant 1$ (mesh refinement): $\Delta x_2/\Delta x_1 = 1$, 0·99, 2/3, 1/3

expansion and $H' = 1/2$ for mesh contraction. The wavelengths adopted were $2{\cdot}001\Delta x_2$, $4\Delta x_2$ and $8\Delta x_2$ for the 'physical' transmitted wavelength with the mesh expansion and $2{\cdot}001\ \Delta x_1$, $4\Delta x_1$ and $8\Delta x_1$ for the incident wavelength in the case of a mesh contraction. (These tests will be generically referred to as the $2\Delta x$, $4\Delta x$ and $8\Delta x$ experiments.) This selection of wavelengths for mesh expansion and mesh refinement had the twofold advantage of permitting easy visual interpretation as well as avoiding the emergence of complex wave numbers and hence wave damping in space.

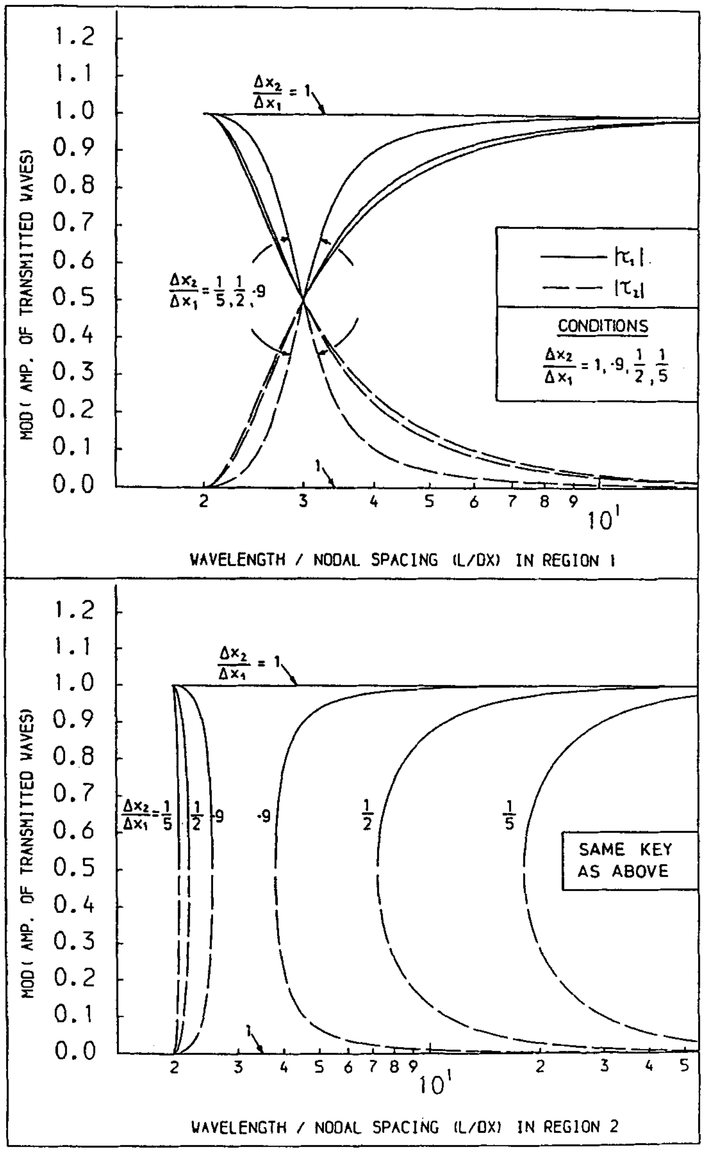

Figure 9. Transmitted waves due to a single change in mesh size (Δx_1 to Δx_2) Crank–Nicolson finite elements applied to the shallow water equations: $\Delta x_2/\Delta x_1 \leqslant 1$ (mesh refinement): $\Delta x_2/\Delta x_1 = 1, 0{\cdot}9, 0{\cdot}5, 0{\cdot}2$

The 'hot-start' initial conditions for the tests were defined by setting $t = 0$ in equations (23)–(28). Since there are two characteristics in the system, two boundary conditions were required, one at each end. The surface elevation was specified at the upstream and downstream boundaries using equations (24) and (26) respectively. The frequency at which these boundaries were oscillated was determined from the dispersion relation for the Crank–Nicolson linear finite element scheme. The results of early tests showed that some disturbances were generated from the ends which tended to obscure the results. The source of the noise is unknown. Although its magnitude was an order smaller than the amplitude of the incident wave, all disturbances emanating from the domain ends for the reflection/transmission tests were windowed out by simply displaying only the central portion of the domain. The numerical tests were stopped before the disturbances penetrated the middle portion of the domain. For example, in a $2\Delta x$ test, 241 nodes were used in the domain but only nodes 81–161 are displayed in the results of the numerical experiments, with the interface located at the middle node (i.e. 121). Similarly, the $4\Delta x$ and $8\Delta x$ tests contained 481 and 961 nodes respectively, with those displayed being nodes 161–321 and 321–641.

A similar format was used to display the results of all the reflection/transmission tests. Output for surface elevation is displayed for the initial conditions as well as at two subsequent times. Regions 1 and 2 are separated by a vertical dashed line which passes through the interfacial node for all three sets of results. The water surface at each node location has been marked with a small circle. Since the finite elements are linear, the small circles have been joined by straight lines to represent the water surface. The mean depth used in all tests was $1/g$(m), which results in a continuum celerity of $1\ \mathrm{m\,s^{-1}}$. The nodal spacing adopted was either 0·5, 1 or 2 m depending on the mesh size ratio and the region being considered. Similarly, the Courant numbers were 0·1, 0·2 or 0·4. Although real for this series of tests in Part I, the reflection and transmission coefficients are generally complex and are recorded in E-format in each figure. The real and imaginary parts are enclosed in brackets. As shown by the analysis, the two reflection coefficients are identically zero for this series of numerical experiments.

Finally, a method was needed in order to highlight any deviations of experimental results produced by the model away from the analytical predictions of equations (24), (26), (28), (38) to (40). The method used was to plot a small triangle to represent the difference between the surface elevation of the model and that of the analysis at each nodal location. Any deviation from the zero or mean water level indicated a discrepancy. In the context of a 'hot-start' experiment ('cold-start' experiments are included in Part II), any non-zero residual indicated a failure of the analysis. The transmission coefficients calculated from equations (39) and (40) were only used for setting up the initial conditions and in calculating the residuals at subsequent times.

After time zero, the solution of the continuity and momentum equations by the numerical model controlled the progress of the incident wave and the two transmitted waves.

In order to demonstrate the results of an incorrect solution in a numerical experiment, one such experiment is displayed in Figure 10. Clearly there is a disturbance which originates from the interface as shown by the non-zero 'residuals' indicated by the small triangles. This result was obtained by swapping the transmission coefficients in equation (26) when defining the initial conditions. That is, the surface elevation in region 2 was (incorrectly) given by

$$\eta(x,t)=\sqrt{(h/g)}\,[\tau_1\,\hat{u}\,\mathrm{e}^{i(\omega t-\sigma_{2b}x)}+\tau_2\,\hat{u}\,\mathrm{e}^{i(\omega t-\sigma_{2a}x)}]$$

instead of the correct solution

$$\eta(x,t)=\sqrt{(h/g)}\,[\tau_1\,\hat{u}\,\mathrm{e}^{i(\omega t-\sigma_{2a}x)}+\tau_2\,\hat{u}\,\mathrm{e}^{i(\omega t-\sigma_{2b}x)}] \tag{26}$$

which is shown later in Figure 16.

3.8. Data used in the numerical experiments

The data used in the six numerical experiments are listed in Table I. The figure numbers in the table refer to the appropriate numerical experiment. In each test the incident wave (i.e. surface elevation) has unit amplitude.

3.9. Results and conclusions of the numerical experiments

The results for the three tests on mesh expansion are displayed in Figures 11–13, while those for the mesh refinement are given in Figures 14–16. In each test it is seen that the analysis has

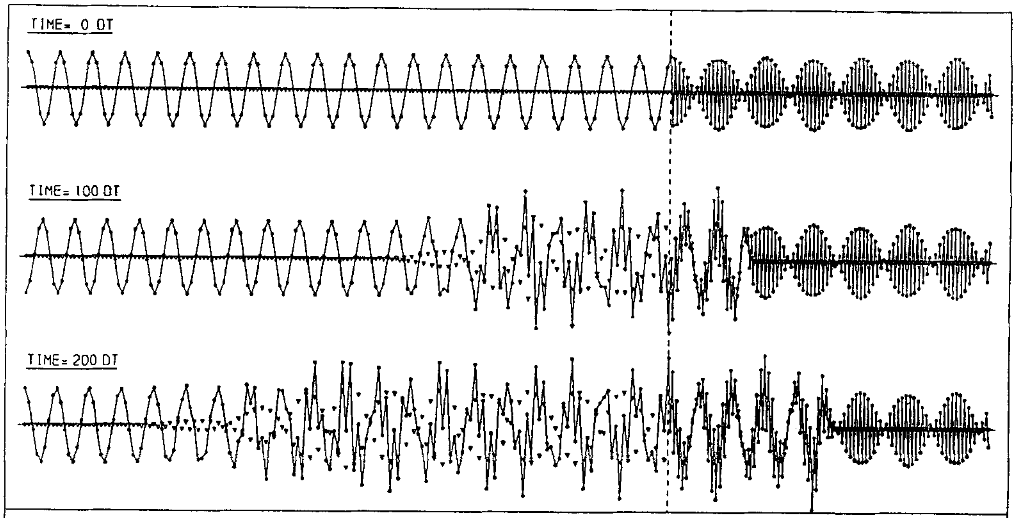

TEST CONDITIONS , DT= 0.2 (S) , CELERITY= 1.00 (M/S) , MEAN DEPTH=1/9.81 (M) CONSISTENT MASS LINEAR ELEMENTS

▿ DENOTES THE RESIDUAL = NUMERICAL SOLUTION FROM MODEL - NUMERICAL PREDICTION FROM ANALYSIS
LHS REGION , DX= 1.0 (M) , COURANT NO.= 0.20, L/DX= 8.0000, REFLECTION COEFFICIENT=(0.00000E00 , 0.00000E00)
RHS REGION , DX= 0.5 (M) , COURANT NO.= 0.40, L/DX=16.0343, TRANSMISSION COEFFICIENT=(0.42231E-01 , 0.00000E00)
L/DX= 2.0878, TRANSMISSION COEFFICIENT=(0.95777E00 , 0.00000E00)

EXPERIMENTS FOR WAVE REFLECTIONS DUE TO A CHANGE IN MESH SIZE FOR THE SHALLOW WATER EQUATIONS

Figure 10. Mesh refinement test showing a disturbance emanating from the interface which is due to the incorrect amplitudes of the two transmitted waves—waves present: incident wave ($8{\cdot}0000\Delta x_1$) and two transmitted waves ($2{\cdot}0878\Delta x_2$ and $16{\cdot}0343\Delta x_2$)

Table I. Data for numerical experiments on wave reflection and transmission; H' is the mesh size ratio and N_x is the dimensionless wavelength

	$H'=2$	$H'=0{\cdot}5$
$N_x=2$	$L_{2a}/\Delta x_2=2{\cdot}0010$ $L_{1a}/\Delta x_1=2{\cdot}0005$ $L_{2b}/\Delta x_2=1334$ $\tau_1=1{\cdot}0000$ $\tau_2=-1{\cdot}4\times10^{-6}$ $\beta_1=\beta_2=0$ (Figure 11)	$L_{1a}/\Delta x_1=2{\cdot}0010$ $L_{2a}/\Delta x_2=2{\cdot}0005$ $L_{2b}/\Delta x_2=2668$ $\tau_1=1{\cdot}0000$ $\tau_2=1{\cdot}4\times10^{-6}$ $\beta_1=\beta_2=0$ (Figure 14)
$N_x=4$	$L_{2a}/\Delta x_2=4{\cdot}0000$ $L_{1a}/\Delta x_1=8{\cdot}3617$ $L_{2b}/\Delta x_2=2{\cdot}5152$ $\tau_1=1{\cdot}4014$ $\tau_2=-0{\cdot}4014$ $\beta_1=\beta_2=0$ (Figure 12)	$L_{1a}/\Delta x_1=4{\cdot}0000$ $L_{2a}/\Delta x_2=8{\cdot}3617$ $L_{2b}/\Delta x_2=2{\cdot}1816$ $\tau_1=0{\cdot}7774$ $\tau_2=0{\cdot}2226$ $\beta_1=\beta_2=0$ (Figure 15)
$N_x=8$	$L_{2a}/\Delta x_2=8{\cdot}0000$ $L_{1a}/\Delta x_1=16{\cdot}0343$ $L_{2b}/\Delta x_2=2{\cdot}1914$ $\tau_1=1{\cdot}0461$ $\tau_2=-0{\cdot}0461$ $\beta_1=\beta_2=0$ (Figure 13)	$L_{1a}/\Delta x_1=8{\cdot}0000$ $L_{2a}/\Delta x_2=16{\cdot}0343$ $L_{2b}/\Delta x_2=2{\cdot}0878$ $\tau_1=0{\cdot}9578$ $\tau_2=0{\cdot}0422$ $\beta_1=\beta_2=0$ (Figure 16)

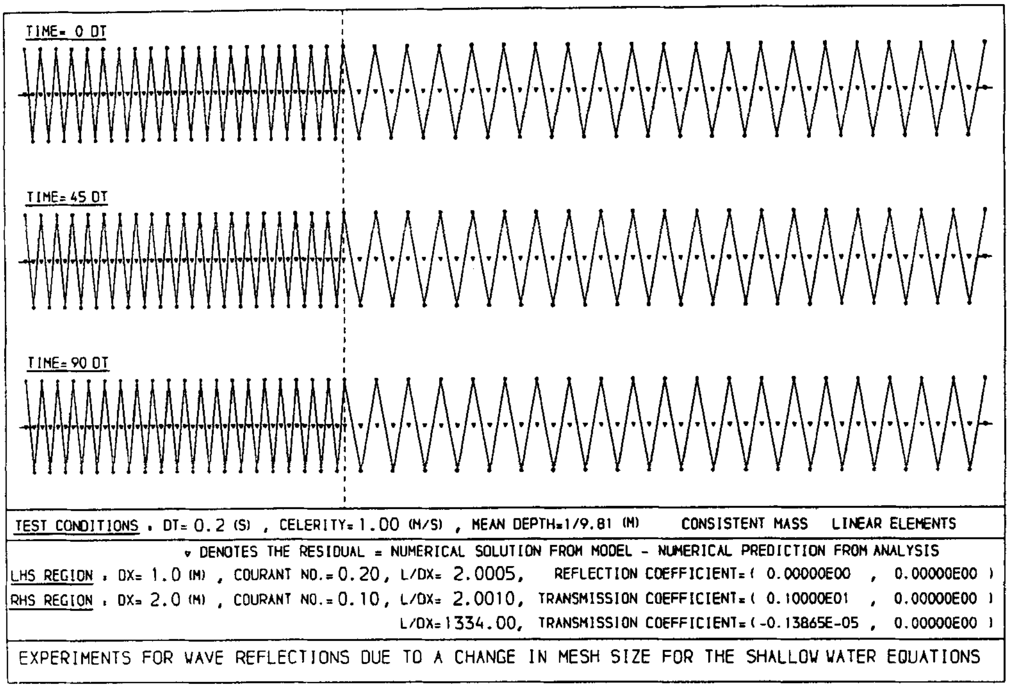

Figure 11. Mesh expansion—waves present: incident wave ($2{\cdot}0005\Delta x_1$) and two transmitted waves ($2{\cdot}0010\Delta x_2$ and $1334\Delta x_2$)

successfully predicted the model results since the residuals, as identified by the small triangles, are everywhere zero. This confirms the general conclusions of there being no reflected waves whatsoever and two transmitted waves present in the downstream region.

3.9.1. Mesh expansion experiments. In Figure 11 for mesh expansion, the $2\Delta x_1$ wave in region 1 is largely unaffected by the change in nodal spacing from one region to the next. The physical transmission coefficient is practically unity, while τ_2, which is associated with the very long wavelength of $1334\Delta x_2$, is almost zero. An interesting point about this test is that while the incident and transmitted waves are effectively stationary, the energy flux is from region 2 to region 1 or from the transmitted wave to the incident wave.

Figure 12 shows how an $8{\cdot}36\Delta x_1$ wave impinging on the interface of a mesh expansion gives rise to a $4{\cdot}0\Delta x_2$ transmitted wave with a transmission coefficient (τ_1) of 1·401 and a $2{\cdot}515\Delta x_2$ complementary wave with a transmission coefficient (τ_2) of $-0{\cdot}401$. The surface elevation in region 2 appears somewhat chaotic but is the result of the superposition of the two transmitted waves. With the generally larger waves appearing in region 2 than for the incident wave in region 1, it appears that energy is being created. This is not the case, however, since the complementary transmitted wave is in fact carrying energy towards the interfacial node rather than away from it.

When the incident wavelength is increased to a $16{\cdot}03\Delta x_1$ wave (see Figure 13), it is evident that the change in mesh size is becoming invisible or insignificant as far as the incident wave is concerned. The reason for this is that the amplitude of the complementary transmitted wave (τ_2) is only 5% of that of the incident wave. The incident wave therefore passes from region 1 to region 2

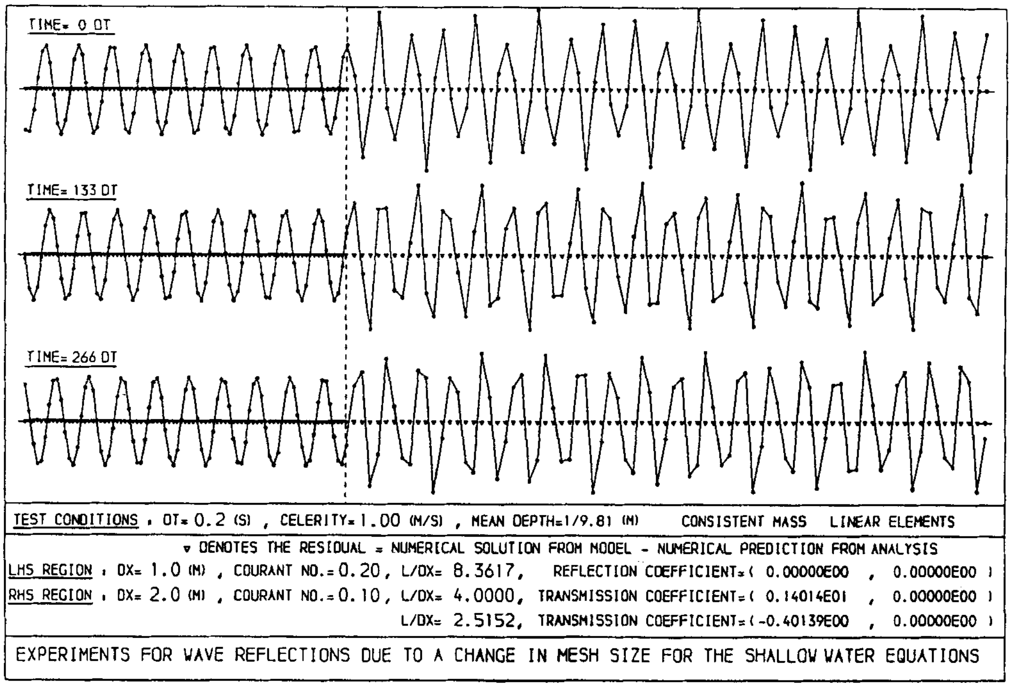

```
TEST CONDITIONS , DT= 0.2 (S) , CELERITY= 1.00 (M/S) , MEAN DEPTH=1/9.81 (M)     CONSISTENT MASS   LINEAR ELEMENTS
           ▽ DENOTES THE RESIDUAL = NUMERICAL SOLUTION FROM MODEL - NUMERICAL PREDICTION FROM ANALYSIS
LHS REGION , DX= 1.0 (M) , COURANT NO.=0.20, L/DX= 8.3617,   REFLECTION COEFFICIENT=( 0.00000E00  ,  0.00000E00 )
RHS REGION , DX= 2.0 (M) , COURANT NO.=0.10, L/DX= 4.0000, TRANSMISSION COEFFICIENT=( 0.14014E01  ,  0.00000E00 )
                                             L/DX= 2.5152, TRANSMISSION COEFFICIENT=(-0.40139E00  ,  0.00000E00 )
EXPERIMENTS FOR WAVE REFLECTIONS DUE TO A CHANGE IN MESH SIZE FOR THE SHALLOW WATER EQUATIONS
```

Figure 12. Mesh expansion—waves present: incident wave ($8{\cdot}3617\Delta x_1$) and two transmitted waves ($4{\cdot}0000\Delta x_2$ and $2{\cdot}5152\Delta x_2$)

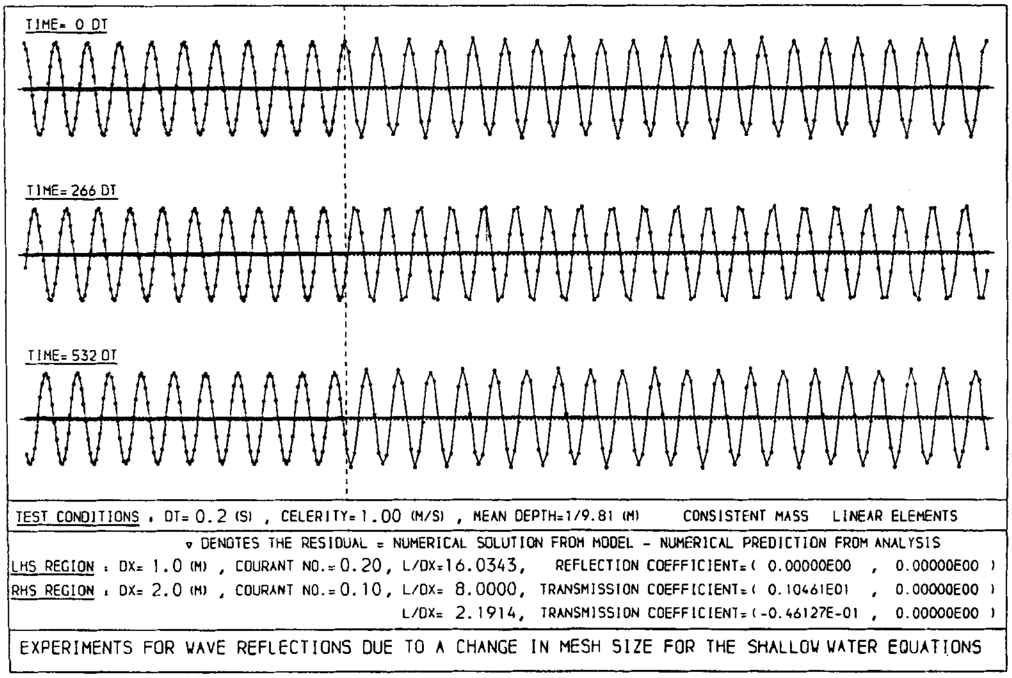

```
TEST CONDITIONS , DT= 0.2 (S) , CELERITY= 1.00 (M/S) , MEAN DEPTH=1/9.81 (M)     CONSISTENT MASS   LINEAR ELEMENTS
           ▽ DENOTES THE RESIDUAL = NUMERICAL SOLUTION FROM MODEL - NUMERICAL PREDICTION FROM ANALYSIS
LHS REGION : DX= 1.0 (M) , COURANT NO.=0.20, L/DX=16.0343,   REFLECTION COEFFICIENT=( 0.00000E00  ,  0.00000E00 )
RHS REGION , DX= 2.0 (M) , COURANT NO.=0.10, L/DX= 8.0000, TRANSMISSION COEFFICIENT=( 0.10461E01  ,  0.00000E00 )
                                             L/DX= 2.1914, TRANSMISSION COEFFICIENT=(-0.46127E-01 ,  0.00000E00 )
EXPERIMENTS FOR WAVE REFLECTIONS DUE TO A CHANGE IN MESH SIZE FOR THE SHALLOW WATER EQUATIONS
```

Figure 13. Mesh expansion—waves present: incident wave ($16{\cdot}0343\Delta x_1$) and two transmitted waves ($8{\cdot}0000\Delta x_2$ and $2{\cdot}1914\Delta x_2$)

relatively unaffected—its wavelength and amplitude change from 16·03Δx_1 and 1·00 in region 1 to 8·00Δx_2 = 16·00Δx_1 and 1·05 in region 2.

For mesh expansions, the extrema in the water surface elevation in region 2 were generally greater or equal to those of the incident wave. For mesh contractions, however, the opposite is true due to the magnitude of both transmission coefficients being smaller than unity.

3.9.2. Mesh contraction experiments. Figure 14 for a mesh contraction is very similar to Figure 11 for a mesh expansion. Once again the 2Δx_1 wave is practically unaffected by the change in nodal spacing between the two regions.

When a 4Δx_1 wave (see Figure 15) impinges on a mesh contraction, an 8·36Δx_2 transmitted wave with a transmission coefficient (τ_1) of 0·777 emerges along with its complement, i.e. a 2·182Δx_2 transmitted wave with a transmission coefficient (τ_2) of 0·223. The generally ragged appearance of the water surface in region 2 is due to the presence of the shorter complementary wave, which transports energy back towards the interface.

Figure 16 indicates how the halving of the nodal spacing presented little obstacle to an incident 8Δx_1 wave, with the amplitude of the aliased transmitted (τ_2) wave being 4% of that of the incident wave.

3.10. *Energy flux across the interface*

Bazant[6] investigated the energy flux across the interface of two regions for the wave equation finite element scheme. The governing equation was the second-order wave equation representing the propagation of waves in a 1D elastic medium such as a string. The energy flux or power

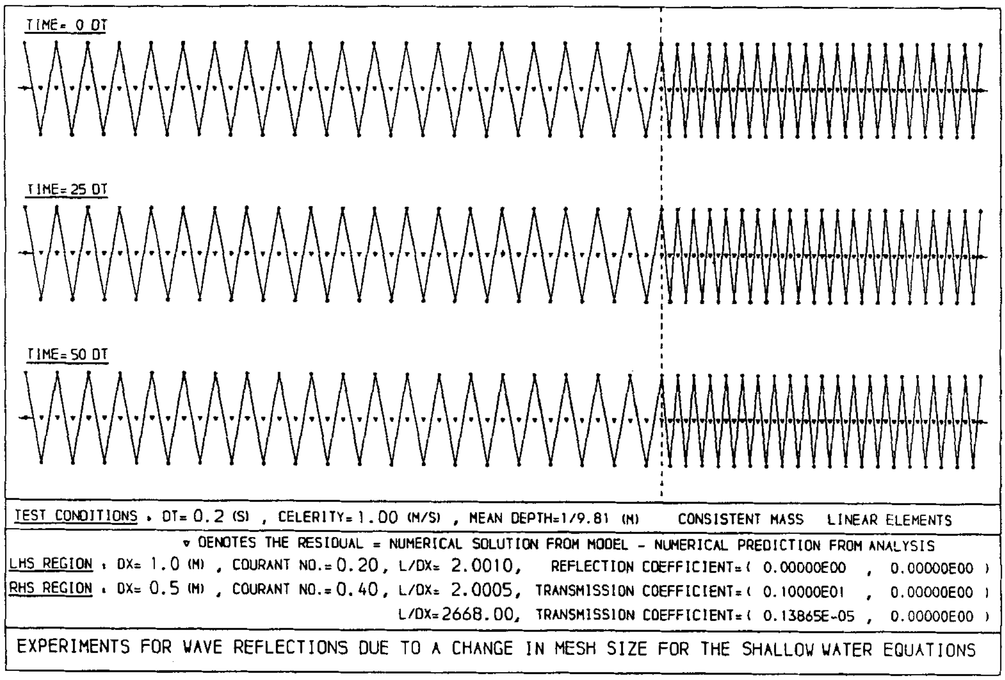

Figure 14. Mesh refinement—waves present: incident wave (2·0010Δx_1) and two transmitted waves (2·0005Δx_2 and 2668Δx_2)

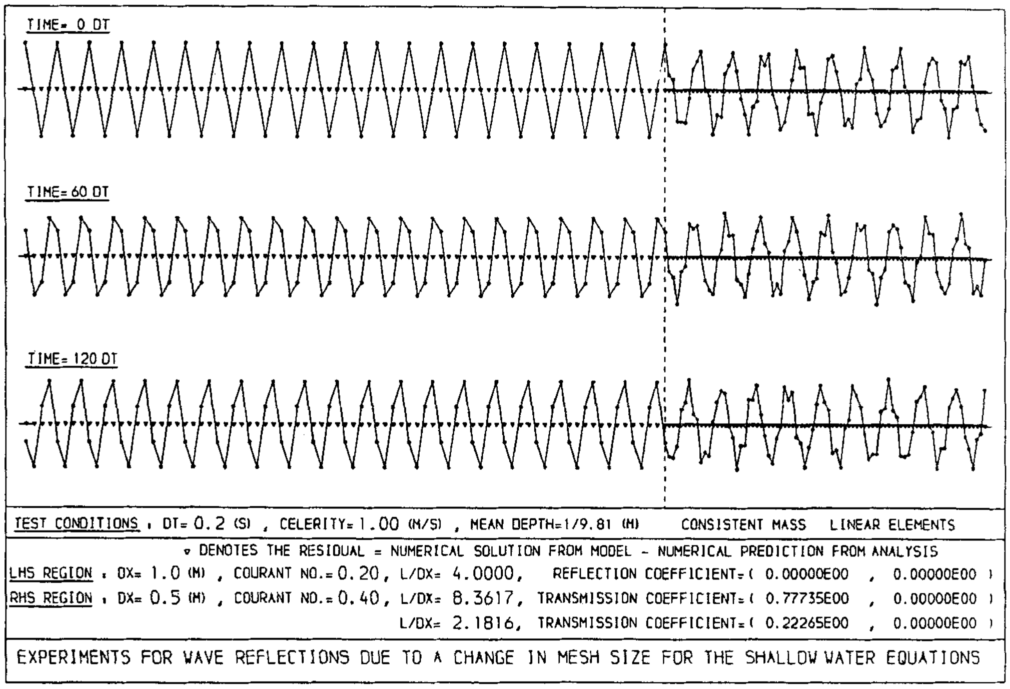

TEST CONDITIONS , DT= 0.2 (S) , CELERITY= 1.00 (M/S) , MEAN DEPTH=1/9.81 (M) CONSISTENT MASS LINEAR ELEMENTS

▿ DENOTES THE RESIDUAL = NUMERICAL SOLUTION FROM MODEL - NUMERICAL PREDICTION FROM ANALYSIS
LHS REGION , DX= 1.0 (M) , COURANT NO.= 0.20, L/DX= 4.0000, REFLECTION COEFFICIENT= (0.00000E00 , 0.00000E00)
RHS REGION , DX= 0.5 (M) , COURANT NO.= 0.40, L/DX= 8.3617, TRANSMISSION COEFFICIENT= (0.77735E00 , 0.00000E00)
L/DX= 2.1816, TRANSMISSION COEFFICIENT= (0.22265E00 , 0.00000E00)

EXPERIMENTS FOR WAVE REFLECTIONS DUE TO A CHANGE IN MESH SIZE FOR THE SHALLOW WATER EQUATIONS

Figure 15. Mesh refinement—waves present: incident wave ($4{\cdot}0000\Delta x_1$) and two transmitted waves ($8{\cdot}3617\Delta x_2$ and $2{\cdot}1816\Delta x_2$)

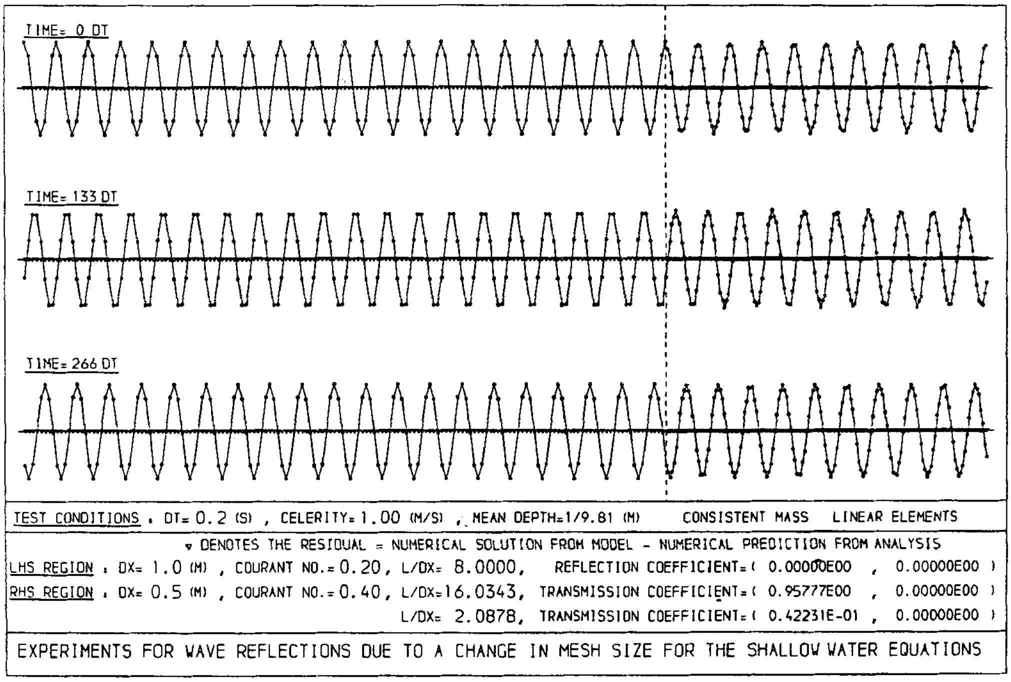

TEST CONDITIONS , DT= 0.2 (S) , CELERITY= 1.00 (M/S) , MEAN DEPTH=1/9.81 (M) CONSISTENT MASS LINEAR ELEMENTS

▿ DENOTES THE RESIDUAL = NUMERICAL SOLUTION FROM MODEL - NUMERICAL PREDICTION FROM ANALYSIS
LHS REGION , DX= 1.0 (M) , COURANT NO.= 0.20, L/DX= 8.0000, REFLECTION COEFFICIENT= (0.00000E00 , 0.00000E00)
RHS REGION , DX= 0.5 (M) , COURANT NO.= 0.40, L/DX=16.0343, TRANSMISSION COEFFICIENT= (0.95777E00 , 0.00000E00)
L/DX= 2.0878, TRANSMISSION COEFFICIENT= (0.42231E-01 , 0.00000E00)

EXPERIMENTS FOR WAVE REFLECTIONS DUE TO A CHANGE IN MESH SIZE FOR THE SHALLOW WATER EQUATIONS

Figure 16. Mesh refinement—waves present: incident wave ($8{\cdot}0000\Delta x_1$) and two transmitted waves ($16{\cdot}0343\Delta x_2$ and $2{\cdot}0878\Delta x_2$)

associated with a wave was derived as the product of the nodal force from the let (i.e. the sum of the elastic and inertial forces on a node) and the velocity of the node. The expression derived was only valid for $\Delta t \rightarrow 0$ since the rate of work cannot be defined exactly for a finite time step. The dependent variables were the nodal displacements, and since the velocity in the energy flux calculation was calculated as the time derivative of the nodal displacement, it could not be defined exactly for finite Δt. When the energy fluxes associated with the incident, reflected and transmitted waves were included, it was shown that there was an energy flux balance across the interfacial node.

In a similar manner, the conservation of energy was examined for the Crank–Nicolson linear finite element scheme, but this investigation was based on the concept of group velocity. The energy flux was calculated as the product of group velocity (which can be defined for finite Δt) and energy intensity.

In region 1 and at the interface where $x \leqslant 0$, we have from equations (23) and (24), with $\beta_1 = \beta_2 = 0 + 0\mathrm{i}$ substituted,

$$u(x, t) = \hat{u}\mathrm{e}^{\mathrm{i}(\omega t - \sigma_{1a} x)}, \tag{41}$$

$$\eta(x, t) = \sqrt{(h/g)}\, \hat{u}\, \mathrm{e}^{\mathrm{i}(\omega t - \sigma_{1a} x)}, \tag{42}$$

and in region 2 and at the interface where $x > 0$,

$$u(x, t) = \tau_1 \hat{u}\, \mathrm{e}^{\mathrm{i}(\omega t - \sigma_{2a} x)} + \tau_2 \hat{u}\, \mathrm{e}^{\mathrm{i}(\omega t - \sigma_{2b} x)}, \tag{43}$$

$$\eta(x, t) = \sqrt{(h/g)}(\tau_1 \hat{u}\, \mathrm{e}^{\mathrm{i}(\omega t - \sigma_{2a} x)} - \tau_2 \hat{u}\, \mathrm{e}^{\mathrm{i}(\omega t + \sigma_{2b} x)}), \tag{44}$$

where

$\gamma_{1a} = \sigma_{1a}\Delta x_1$ dimensionless wave number of the incident wave

$\gamma_{2a} = \sigma_{2a}\Delta x_2$ dimensionless wave number of the 'physical' transmitted wave

$\gamma_{2b} = \sigma_{2b}\Delta x_2$ dimensionless wave number of the 'non-physical' transmitted wave.

Energy is conserved if the energy flux due to the incident wave is equal to that due to the sum of the two transmitted waves. The energy flux is the product of the group velocity and the energy intensity. A general expression will now be obtained for the energy flux associated with a wave.

The kinetic energy density (KE) averaged over the length of an element (Δx) is

$$\mathrm{KE} = \frac{\rho}{2\Delta x}\int_0^{\Delta x} u^2\, \mathrm{d}x, \tag{45}$$

but in the finite element theory,

$$u = N_j u_j + N_{j+1} u_{j+1}, \tag{46}$$

where $N_j = 1 - x/\Delta x$ and $N_{j+1} = x/\Delta x$. Substituting equation (46) into (45) gives

$$\mathrm{KE} = \frac{\rho}{6}(u_j^2 + u_j u_{j+1} + u_{j+1}^2), \tag{47}$$

but

$$u_j = \hat{u}\, \mathrm{Re}(\mathrm{e}^{i(\omega t - \sigma j \Delta x)}) \tag{48}$$

where Re ( ) denotes the taking of the real part. Substitution of equation (48) into (47) leads to

$$\mathrm{KE} = \frac{\rho\hat{u}^2}{6}[\sin^2(\omega t - \sigma j\Delta x) + \sin(\omega t - \sigma j\Delta x) + \sin(\omega t - \sigma j\Delta x)\sin(\omega t - \sigma j\Delta x - \gamma)], \tag{49}$$

where $\gamma = \sigma \Delta x$. The kinetic energy density can then be averaged over a wave period to give

$$\overline{\mathrm{KE}} = \frac{1}{T}\int_0^T \mathrm{KE}\,\mathrm{d}t = \frac{\rho \hat{u}^2}{12}(2+\cos\gamma)$$

after substituting equation (49).

Since there is equipartition of kinetic and potential energy over the wave period in a linear non-dissipative system, the total energy density is

$$\bar{E}_{\mathrm{tot}} = 2\,\overline{\mathrm{KE}} = \frac{\rho \hat{u}^2}{6}(2+\cos\gamma). \tag{50}$$

The numerical group velocity ratio is found from the dispersion relation (equation (11)) and is given by

$$C_{\mathrm{gnum}} = \frac{\partial \omega}{\partial \sigma} = \frac{3c(1+2\cos\gamma)}{(\cos\gamma+2)^2 + (1{\cdot}5\not{C}\sin\gamma)^2} = \cos^2(\omega\Delta t)\frac{3c(1+2\cos\gamma)}{(2+\cos\gamma)^2}. \tag{51}$$

Therefore the time- and space-averaged energy flux for a wave with amplitude $\hat{u}$ is given by

$$E_{\mathrm{flux}} = \bar{E}_{\mathrm{tot}}\,C_{\mathrm{gnum}} = \frac{\rho c \hat{u}^2}{2}\left(\frac{1+2\cos\gamma}{2+\cos\gamma}\right)\cos^2(\omega\Delta t). \tag{52}$$

Using $\hat{u} = \sqrt{(g/h)}\hat{\eta}$ and equation (52), the energy fluxes associated with the unit incident wave and two transmitted waves of equations (42) and (44) are

$$E_{\mathrm{flux,incident}} = \frac{\rho c g}{2h}\left(\frac{1+2\cos\gamma_{1\mathrm{a}}}{2+\cos\gamma_{1\mathrm{a}}}\right)\cos^2(\omega\Delta t),$$

$$E_{\mathrm{flux,}\,\underset{1}{\mathrm{transmitted}}} = \frac{\rho\tau_1^2 c g}{2h}\left(\frac{1+2\cos\gamma_{2\mathrm{a}}}{2+\cos\gamma_{2\mathrm{a}}}\right)\cos^2(\omega\Delta t),$$

$$E_{\mathrm{flux,}\,\underset{2}{\mathrm{transmitted}}} = \frac{\rho\tau_2^2 c g}{2h}\left(\frac{1+2\cos\gamma_{2\mathrm{b}}}{2+\cos\gamma_{2\mathrm{b}}}\right)\cos^2(\omega\Delta t).$$

Energy is conserved if the expression equating the incident wave energy flux to the sum of the two transmitted wave energy fluxes is satisfied. This implies

$$\frac{\rho c}{2}\left(\frac{1+2cos\,\gamma_{1\mathrm{a}}}{2+\cos\gamma_{1\mathrm{a}}}\right) = \frac{\rho\tau_1^2 c}{2}\left(\frac{1+2\cos\gamma_{2\mathrm{a}}}{2+\cos\gamma_{2\mathrm{a}}}\right) + \frac{\rho\tau_2^2 c}{2}\left(\frac{1+2\cos\gamma_{2\mathrm{b}}}{2+\cos\gamma_{2\mathrm{b}}}\right). \tag{53}$$

When the expression above is simplified using the dispersion relation (11) and equations (39) and (40), equation (53) is valid and energy is conserved.

4. CONCLUSIONS

The analysis has shown that two transmitted waves arise when an incident wave impinges on a change in mesh size for the Crank–Nicolson linear finite element scheme. The magnitude and phasing of the transmitted waves with respect to the incident wave have been quantified and the results verified by ‘hot-start’ experiments.

REFERENCES

1. W. C. Thacker, 'Irregular-grid finite difference techniques for storm surge calculations for curving coastlines', in J. C. J. Nihoul (ed.), *Marine Forecasting (Predictability and Modelling in Ocean Hydrodynamics), Proc. 10th Int. Liege Coll. on Ocean Hydrodynamics,* Elsevier Oceanography Series No. 25, 1979.
2. R. R. Boericke and D. W. Hall, 'Hydraulics and thermal dispersion in an irregular estuary', *J. Hydraul. Div., Proc. ASCE*, **100,** 85–102. (1974).
3. N. A. Phillips and J. Shukla, 'On the strategy of combining coarse and fine grid meshes in numerical weather prediction', *J. Appl. Meteorol.*, **12,** 763–770 (1973).
4. A. Langerak, M. A. M. de Ras and J. J. Leendertse, 'Adjustment and verification of the Randdelta II model,' *Proc. 16th Coastal Engineering Conf., Vol. 1,* Hamburg 27 August–3 September 1978.
5. Hydraulics Research Station, Wallingford, 'Patchwork models', *Annual Report 1980,* Department of the Environment, London, HMSO, 1980.
6. Z. P. Bazant, 'Spurious reflection of elastic waves in non-uniform finite element grids', *Comput. Methods Appl. Mech. Eng.*, **16,** 91–100 (1978).
7. Z. P. Bazant and Z. Celep, 'Spurious reflection of elastic waves in non-uniform meshes of constant and linear strain FEs', *Comput. Struct.*, **15,** 451–459 (1982).
8. Z. Celep and Z. P. Bazant, 'Spurious reflection of elastic waves due to gradually changing FE size', *Int. j. numer. methods eng.*, **19,** 631–646 (1983).
9. R. Vichnevetsky, 'Invariance theorems concerning reflection at numerical boundaries', *J. Comput. Phys.*, **63,** 268–282 (1986).
10. L. N. Trefethen, 'Wave propagation and stability for finite difference schemes', *Ph.D. Thesis*, Stanford University, May 1982; also *Department of Computer Science Report No. STAN-CS-82-905,* 1982.
11. R. Vichnevetsky, 'Wave propagation analysis of difference schemes for hyperbolic equations: a review', *Int. j. numer. methods fluids*, **7,** 409–452 (1987).
12. B. Worthington, Private communication, 1982.
13. H. Lamb, *Hydrodynamics*, Dover, 1972
14. I. A. Svendsen and I. G. Jonsson, 'Hydrodynamics of coastal regions', Den Private Ingeniorfond, Technical University of Denmark, Lyngby, 1980.
15. G. W. Platzman, 'Some response characteristics of finite element tidal models', *J. Comput. Phys.*, **40,** 36–63 (1981).